5-2015

Direct Electrical Arc Ignition of Hybrid Rocket Motors

Michael I. Judson Jr.
Utah State University

DIRECT ELECTRICAL ARC IGNITION OF HYBRID ROCKET MOTORS

by

Michael I. Judson Jr

A thesis submitted in partial fulfillment
of the requirements for the degree

of

MASTER OF SCIENCE

in

Aerospace Engineering

Approved:

_____   _____
Dr. Stephen Whitmore   Dr. Rees Fullmer
Major Professor   Committee Member

_____   _____
Dr. David Geller   Dr. Mark McLellan
Committee Member   Vice President for Research and
                                         Dean of the School of Graduate Studies

UTAH STATE UNIVERSITY
Logan, Utah

2015

Abstract

Direct Electrical Arc Ignition of Hybrid Rocket Motors

by

Michael I. Judson Jr, Master of Science

Utah State University, 2015

Major Professor: Dr. Stephen Whitmore
Department: Mechanical and Aerospace Engineering

Hybrid rockets motors provide distinct safety advantages when compared to tra-
ditional liquid or solid propellant systems, due to the inherent stability and relative
inertness of the propellants prior to established combustion. As a result of this inher-
ent propellant stability, hybrid motors have historically proven difficult to ignite. State
of the art hybrid igniter designs continue to require solid or liquid reactants distinct
from the main propellants. These ignition methods however, reintroduce to the hybrid
propulsion system the safety and complexity disadvantages associated with traditional
liquid or solid propellants. The results of this study demonstrate the feasibility of a
novel direct electrostatic arc ignition method for hybrid motors. A series of small pro-
totype stand-alone thrusters demonstrating this technology were successfully designed
and tested using Acrylonitrile Butadiene Styrene (ABS) plastic and Gaseous Oxygen
(GOX) as propellants. Measurements of input voltage and current demonstrated that
arc-ignition will occur using as little as 10 watts peak power and less than 5 joules total
energy. The motor developed for the stand-alone small thruster was adapted as a gas
generator to ignite a medium-scale hybrid rocket motor using nitrous oxide /and HTPB
as propellants. Multiple consecutive ignitions were performed. A large data set as well as
a collection of development 'lessons learned' were compiled to guide future development

and research. Since the completion of this original groundwork research, the concept has been developed into a reliable, operational igniter system for a 75mm hybrid motor using both gaseous oxygen and liquid nitrous oxide as oxidizers. A development map of the direct spark ignition concept is presented showing the flow of key lessons learned between this original work and later follow on development.

(89 pages)

Public Abstract

Direct Electrical Arc Ignition of Hybrid Rocket Motors

by

Michael I. Judson Jr, Master of Science

Utah State University, 2015

Major Professor: Dr. Stephen Whitmore
Department: Mechanical and Aerospace Engineering

Hybrid rockets motors provide distinct safety advantages when compared to tra-
ditional liquid or solid propellant systems, due to the inherent stability and relative
inertness of the propellants prior to established combustion. Hybrid motors however
have historically proven difficult to ignite. State of the art hybrid igniter designs con-
tinue to require solid or liquid reactants distinct from the main propellants. These
ignition methods reintroduce to the hybrid propulsion system the safety and complexity
disadvantages associated with traditional liquid or solid propellants. The results of this
study demonstrates the feasibility of a novel direct electrostatic arc ignition method for
hybrid motors. A series of small prototype stand-alone thrusters demonstrating this
technology were successfully designed and tested during this work, including a small gas
generator motor used for multiple sucessive ignitions of a medium-scale hybrid rocket
motor. These tests resulted in a large data set, and a collection of development 'lessons
learned', that were compiled as a guide for future development and research. Since
the completion of this research, the direct electrostatic arc ignition concept has been
developed into a reliable, operational igniter system for a 75mm hybrid motor.

(89 pages)

Acknowledgments

I would like to thank my adviser, Dr. Stephen Whitmore, whose advice, guidance, and enthusiasm facilitated my work and allowed me to gain invaluable experience. I deeply appreciate the support of my comitee members, Dr. David Geller and Dr. Rees Fulmer.

I also owe much appreciation to the other members of the hybrid motor research group, who established much of the test infrastructure and processes that made my research possible. Shannon Eilers, Zach Peterson, Matthew Wilson, Jonathan McCulley, and Andrew Bath worked diligently to build the test capabilities that currently exist.

The construction of key pieces of hardware for this project were made possible through the skill of our machinist Terry Zolinger. I am also very greatful to Randy Chesley who kindly opened the test cell for testing on multiple early weekend mornings.

Above all I am greatful to my wife, Sarah, whose patience and encouragement during my research were nothing short of heroic.

<div align="right">Michael Judson</div>

Contents

List of Tables

List of Figures

Nomenclature

HTPB	Hydroxyl-Terminated Polybutadiene
AP	Ammonium Perchlorate
ISP	Specific Impulse
TRL	Technology Readiness Level
MH##	Microhybrid test designation numbering scheme
FDM	Fused Deposition Modeling
ABS	Acrylonitrile Butadiene Styrene
CB	Carbon Black
CEA	Chemical Equilibrium with Applications
HVPS	High Voltage Power Supply
Vsp	Specific Volume

Chapter 1

Introduction and Background

1.1 Research Motivation

Hybrid rocket ignition has historically posed unique challenges, with state of the art solutions continuing to involve carrying reactive materials distinct from the main propellants. In many cases the ignition process may negate much of the hybrid motor's inherent simplicity or safety and may deny the ability to restart the motor. This study seeks to demonstrate a restartable, miniaturized, hybrid motor using electrostatic arc ignition which may be used as the basis for either a stand-alone thruster or as a hot gas generator (igniter) for the ignition of larger motors. The concept for this microhybrid motor and ignition system consists of electrode pathways embedded into the hybrid fuel grain, between which a high voltage spark is formed. The spark ablates solid fuel into the oxidizer and provides the initiation energy required to ignite the propellants. This initial combustion causes further fuel ablation leading to a self-sustaining reaction.

This ignition concept allows for hybrid motor systems which fully realize the safety, simplicity, and restartablility advantages which are often cited in connection with hybrid motors [5]. Because the concept uses a spark to directly ignite the main propellants, no additional igniter reactants are required, and a single-flow-path ignition system is possible. Motor restarts are limited only by the quantity of propellants carried, and additional fluid handling and conditioning systems are largely avoided.

1.2 Background on Rocket Systems

Chemical rockets encompass the broad class of impulsive propulsion devices that use stored chemical energy to heat propellant gasses and eject them at high speed through a nozzle. Typical rockets consist of a combustion chamber in which the oxidizer and

fuel elements are mixed and burned creating high energy gas flow. This gas is allowed to escape through a convergent-divergent nozzle accelerating the flow to high speed.

Within chemical rockets three main categories exist, grouped primarily by the phase at which the various propellant constituents are stored. Solid propellant motors store an oxidizer and fuel element in a premixed solid grain within the combustion chamber. Liquid rockets store one or more propellants in tanks external to the combustion chamber. During operation these propellants are forced into the combustion chamber where they are allowed to react. Hybrid rockets combine aspects of both liquids and solids, with typical implementations using a solid fuel grain stored within the combustion chamber and a liquid oxidizer stored in a tank external to the motor. Upon ignition, the liquid oxidizer is injected into the combustion chamber where it reacts with the fuel element. Each of these three categories carries advantages and disadvantages to be described in the following sections.

1.2.1 Solid Motors

Solid rocket motors are inherently mechanically simpler than other propellant combinations, removing the need for fluid handling valves, tanks, pressurization systems, and injectors. The propellants can also typically be stored for long periods of time both on the ground as well as in the space environment. However, because the oxidizer and fuel are premixed, solid fuel grains are subject to the Hazards of Electromagnetic Radiation to Ordinance (HERO) [6] and great caution is required in their transport and handling. This typically leads to increased cost and regulatory overhead. Solid rocket performance will achieve specific impulse (ISP) up to 280-290 s in vacuum for a well optimized hydroxyl terminated polybutadiene (HTPB) and ammonium perchlorate (AP) composite propellant [7]. Because solid motors can be optimized to give large thrust from a compact form factor, they have found use extensively in missiles. Other typical uses include strap-on or main stage boosters for launch vehicles, apogee kick motors, and ejection/escape systems.

A significant drawback to solid motors is the inability to actively throttle or shutdown and restart the motor in flight. Considerable research has gone into the development of grain designs which produce specific thrust profile over the duration of the burn [7], however such an 'open-loop' method does not allow for a response to measured in-flight conditions. Systems, such as the Hercules M57 Motor used on the Minute Man series of ICBMs, which perform a controlled rupture of the combustion chamber pressure vessel have been developed [8] in order to control the total impulse delivered to the vehicle. However, for missions that require inflight control of the propulsion system the applicability of solids remains limited. Throttling has been attempted using pintle type throat area constriction [9] or through breaking the grain into distinct sections separated by a combustion inhibiting layer [10], though these technologies typically carry a lower TRL and impose additional constraints on the overall vehicle system.

Though attempts have been made at reusable solid motors such, these have had questionable economic and technical benefit, and so typical solid motor system designs are cable of single use only.

1.2.2 Liquid Engines

Liquid engines carry the primary benefit of high performance, controllability, and the possibility for more complete reusability. Because propellant flows can be controlled by valves or pumps, liquids can, in principle, be throttled in a closed loop fashion as well as shutdown and restarted. Highly optimized systems such as the SSME may achieve up to 450 s vacuum ISP [4]. This increase in performance however comes with a corresponding increase in complexity and development costs.

The highest performing liquid propellants are cryogenic and are not long term storable in the space environment. Of the available storable liquid propellants, historically all common implementations have been highly toxic, carcinogenic, corrosive or a combination of more than one of these undesirable characteristics [11]. Because of costs associated with handling these highly dangerous materials [12] investment has been made into so called 'green' propellant combinations, which typically involve nitrous

oxide as the oxidizing agent [13]. These engines, while offering promising alternatives to toxic propellants, typically suffer from lower performance and currently still have lower TRL.

Mono propellant engines are a subset of liquid propulsion systems which use a single liquid component that is decomposed exothermically typically with the use of a catalyst bed. Often catalyst beds require an external heat source, typically an electro-resistive type heater, to raise the catalyst to a sufficient temperature to begin the reaction. Hydrazine or to a lesser extent hydrogen peroxide are the most commonly used propellants. These propellants have the advantage of being space storable. ISP performance is medium, with typical values in the range of 234 s in vacuum. Monopropellant thrusters based in hydrazine have a long flight heritage down to the sub 1 N thrust level [14]. The catalytic decomposition ignition occurs passively simply by opening the main propellant valve thus increasing simplicity and scalability and allowing for reignition capability that is only constrained by available propellant. The technology scales well, though thruster volume and mass properties for very small thrusters are typically dominated by the valve design.

The current state of the art monopropellant fuels are highly toxic, carcinogenic, and/or corrosive and therefor can pose serious safety challenges. This property leads to severely elevated costs associated with the handling operations surrounding vehicles using these propellants. Especially, in the case of small low-cost satellites, these costs, and the requisite infrastructure for safe handling, may be prohibitive [12, 15]. Although procedures are in place to allow hydrazine to be managed safely on tightly controlled military ranges and has flown multiple times on DoD and NASA-owned flight experiments; the toxicity and explosion potential of hydrazine requires extreme handling precautions. Increasingly, with a growing regulatory burden and infrastructure requirements associated with hydrazine transport, storage, servicing, and clean up of accidental releases, operating costs for hydrazine are becoming prohibitive. Extreme handling precautions generally do not favor hydrazine as a propellant for secondary payloads. In 2003 a

study performed by EADS for the European Space Agency (ESA) showed the potential for considerable operational cost savings by simplifying propellant ground handing procedures [15]. Hydrazine also has the disadvantage of offering only modest mass and volumetric efficiency, with Isp ~ 220-240 sec, Vsp ~ 220-240 g-sec/cm3.

1.2.3   Hybrid Motors

Hybrid motors consist of a liquid oxidizer combined with a solid fuel element. In order for mixing of propellants to take place, combustion must be established in the thrust chamber causing pyrolysis of the fuel grain surface. The gaseous pyrolysis products then combine with the oxidizer and combust creating a self-sustaining reaction.

Hybrid motors combine desirable aspects of both solid and liquid propulsion systems along with benefits unique from either of these. Compared with liquid bipropellant engines, hybrids carry a significant simplicity benefit. Because only a single liquid propellant is used, the required liquid feed system is simplified, requiring fewer valves, lines, and tanks. In many ways hybrid systems are more akin to monopropellant liquid engines than bipropellants. Additionally, thrust chamber thermal management is accomplished primarily by the ablation of the solid fuel grain, sometimes supplemented by insulation, avoiding the need for complex regenerative cooling.

Hybrids, in theory, maintain the ability to throttle and restart the motor comparable to liquid engines. One example of hybrid motor throttling was demonstrated successfully by Whitmore, Peterson, and Eilers [16] [17], who deep-throttled a nominal 800-lbf hybrid motor to less than twenty-five percent thrust rating in a closed-loop control system. This provides a significant advantage for systems which require propulsion throttling but where mission constraints make the complexity or safety disadvantages of bi-propellant liquid engines prohibitive.

The primary benefit of hybrid motors however lies in inherent safety. In a hybrid, propellants are stored separately, with one component in a solid state. Because combustion is required to ablate the solid grain and mix the propellants, there is no potential for unburned fuel and oxidizer to mix in a way which would form an explosive mixture. For

the same reason, hybrids are less prone to start-up overpressure events or 'hard-starts' caused by incomplete or delayed ignition. The greatly decreased probability of hard start contributes to the potential for significantly less expensive hybrid motor development when compared to similar sized liquid engines.

Common hybrid motor propellants include Nitrous Oxide or liquid oxygen combined with HTPB rubber or other solid hydrocarbon-based polymers. The most commonly employed fuel is HTPB, a legacy binder left over from solid propulsion development. These propellants are generally safe to handle with established industrial standards, leading to increased safety of ground support operations and decreased costs for development and implementation.

Because of low regression rates of solid fuels used in hybrids, typical motors must be designed with long chamber lengths or increased grain complexity (multiple ports) in order to provide sufficient burning surface area to input sufficient fuel into the combustion gases. Long chamber motors pose packaging issues for systems employing hybrids and shortening though multi-port configurations typically negatively affects effective fuel storage density and dry mass though the increase in fuel residuals. Solutions to the hybrid packaging issue however exists in novel grain designs such as proposed by Eilers [18] and Whitmore et al. [19] or higher regression fuel formulations such as those implemented by Space Propulsion Group [20]. Hybrid systems have also historically suffered from lower performance compared with well optimized liquid and solid systems, with current state of the art motors achieving 250-280s ISP depending on the specific propellant combination [4]. Additionally, for some fuel grain geometries, system effective dry mass is increased by fuel residuals that cannot be effectively burned out of the combustion chamber.

Hybrids have the capability to fill niche applications where safety advantages are weighted more heavily than typical standard performance measures. Because a wide variety of non-toxic, relatively stable, propellants are available for hybrid systems, decreased performance may be traded for increased safety and simplicity.

1.3   Hybrid Propulsion for Small Satellites

One potential application where hybrid advantages may be weighted more heavily than traditional performance measures is in small low cost satellites. A small satellite system may be defined as those with a total (wet) mass less than 500 kg. Small spacecraft continue to be an area of interest to both government and commercial entities [21] [22]. Satellites in the Small Satellite range have the advantage of faster development time frames, lower development and launch costs, increased mission flexibility, and the potential for mission objective risk reduction through distribution of risk among many cooperative spacecraft. The miniaturization of satellite technology presents several challenges however to the subsystem groups that form the basic spacecraft infrastructure. Communication, thermal management, attitude determination and control, and propulsion all require special consideration due to challenges of miniaturization for these spacecraft. With the revolution of lower cost miniaturized electronic systems, a number of commercial ventures are seeking to capitalize on the potential of small satellites.

No dedicated launch vehicle currently exists for small satellites, though a number are in development [23]. Presently, the primary orbital accesses opportunity for this type as space craft exists as a ride share transport as secondary payload on a large traditional launch vehicle. This further complicates the requirements for a small spacecraft propulsion system because especially strict safety requirements are placed on any propulsion unit carried as a secondary payload. Reducing risk for the primary payload will generally take precedent over secondary payload mission considerations, thus any propulsion unit designed for a secondary payload must often make safety the top design priority. Further miniaturization of safe, high performance, micro propulsion units is required to enable many envisioned small sat missions. Requirements specific to propulsion systems carried as a secondary payload include: long term storability, ease and safety of integration with the launch vehicle, and maximizing inertness before and during integration.

A number of potential options exist at various states Technology Readiness Level. No single "Silver Bullet" propulsion system currently covers the requirements of most

mission in the area of small satellites; rather trades must be evaluated to match a propulsion system with the specific requirements for each mission. When evaluating propulsion systems for small satellites, especially those carried as secondary payloads, the trade space of propulsion options is limited.

The relative strengths, weaknesses, and features of the current state of the art propulsion systems informed areas for focus in the development of the microthruster motor and igniter which was explored during this research effort. The electrostatic arc ignition microhybrid concept presented here has applicability for many small satellite missions with the potential for nearly inert long term storage, and a high degree of inherent safety simplicity.

1.4 ABS Plastic as a Hybrid Rocket Fuel

The work presented here has built on recent research at Utah State University which has explored the potential of ABS thermoplastic for use as a hybrid rocket fuel. Whitmore, et al. demonstrated that the thermodynamic performance potential of ABS is nearly equivalent to the most commonly used hybrid fuel, Hydroxyl-Terminated Polybutadiene (HTPB) [24]. This research showed that when used with Nitrous Oxide (N2O), while ABS combustion temperatures are lower when compared to HTPB, the combustion products have a lower molecular weight. This result leads to equivalent characteristic velocity (C*) and specific impulse (ISP) performance when comparing ABS to HTPB. Whitmore, et al. also found that ABS and HTPB regression rates were comparable leading to the possibility of substituting ABS for HTPB without major performance penalties.

When considering manufacture and system level trades, ABS has a number of mechanical and chemical properties that make it attractive over HTPB. Because ABS is a thermoplastic, it can be formed into complex geometries without using a casting process, i.e. using additive manufacturing techniques. ABS is also easily machined after the initial forming processes. For a thermoset like HTPB, complex geometries are restricted by the requirement to remove a mandrel or other tooling used in the casting

processes and post casting shaping is difficult or impossible. Mechanically, ABS is much more rigid and, therefore for some motors, may allow the fuel to provide a significant portion of the motor structure. These advantages made ABS a prime candidate for the igniter developed in this study, allowing for rapid iteration of fuel grain geometries with complex embedded electrode pathways.

1.5 Background on Rocket Ignition Methods

The issue of ignition has historically been one of the key challenges in rocket propulsion development. For systems using mono-propellant or bi-propellant liquids, ignition sequence is especially critical to avoiding catastrophic hard starts. For systems employing multiple motors/engines or performing staging, ignition timing and consistency may be particularly critical to avoid asymmetrical thrust distribution.

The selection of a specific ignition system depends on many attributes of the overall vehicle and propulsion system design. Primary among these considerations is the propellant combination selected. Where possible, an ignition system should avoid introducing additional complexity and minimize additional system dry mass. For these reasons it is often advantageous to select an ignition system that utilizes the propellants and systems already available to the main propulsion system. For hybrid rocket motors, using only the main motor propellants as reactants for the igniter system has proven difficult due to the relative inertness of common hybrid propellant combinations prior to establishing combustion [25].

Historically, many different approaches have been used to ignite rocket motors. These include hypergolic reactants, resistive elements (low voltage), augmented high voltage spark (liquid bi-propellant torch), pyrotechnics, catalyzed monopropellants, and high power plasma arcs. The ignition system proposed here is distinct from any of these previous options in that a high voltage source is used to cause the direct ignition of a solid fuel and fluid oxidizer. In order to highlight the relative strengths of this method a background on rocket ignition is provided in the following discussion.

1.5.1 Ignition vs. Initiation

Ignition of a rocket propulsion system and initiation of combustion are related but subtly different concepts. For the purposes of this discussion initiation will be defined as the event causing the first occurrence of combustion within a subsystem of the propulsion system. Ignition of the rocket will be defined as the initiation of combustion of the main propellant or propellants. Depending on the specific ignition method used, initiation may occur simultaneous with or prior to actual main propellant ignition.

1.5.2 Hypergolic Ignition

Hypergolic igniters use a combination of hypergolic reactants (hypergols) which ignite spontaneously upon contact. In hypergolically ignited motors, initiation of combustion may occur simultaneous with or just prior to main propellant ignition. Common hypergolic propellant combinations include monomethyl hydrazine, hydrazine, and unsymetric dimethlhydrazine paired with Nitrogen Tetroxide or Nitric Acid. Pyrophoric mixtures are a subset of hypergols which spontaneously combust when exposed to oxygen. These include combinations such as the common triethylaluminum –triethylborane (TEA-TEB). Hypergolic combinations may be used in the ignition system only or as the main propellant for the engine. Examples of hypergolicaly ignited engines include the Rocketdyne F1 used on the Saturn V vehicle as well as the SpaceX Merlin engine family [26]. Hypergolic systems have the advantage of providing a simple and highly reliable ignition.

Hypergols have been used as the ignition system for non-hypergolic main propellants by leading the main propellant flow with a 'plug' of a hypergolic of pyrophoric liquid. Propellant systems, such as the Rocketdyne F1 shown in Figure 1.1, have successfully implemented this type of hypergolic ignition by storing hypergolic reactants in the feed line ahead of the main propellant [27]. In such a system, when propellant flow is initiated, the hypergolic reactants are pushed into the chamber ahead of main propellant flow thus igniting the chamber. The ignition system is thus reduced in complexity by removing the need to carefully coordinate the timing of main propellant valves to igniter events.

Because a single event (opening the main propellant valves) directly controls both the igniter flow as well as main propellant flow, the system is made more robust against variability in valve opening and manifold fill times. This approach allows for bipropellant systems to use hypergolic ignition without the need for an additional self-contained fluid systems. However, in hybrid or solid systems attempting to use hypergolic ignition, a separate igniter fluid system is still be required, as hypergols necessarily require a two fluid line system in order to keep the components separated before the desired ignition event.
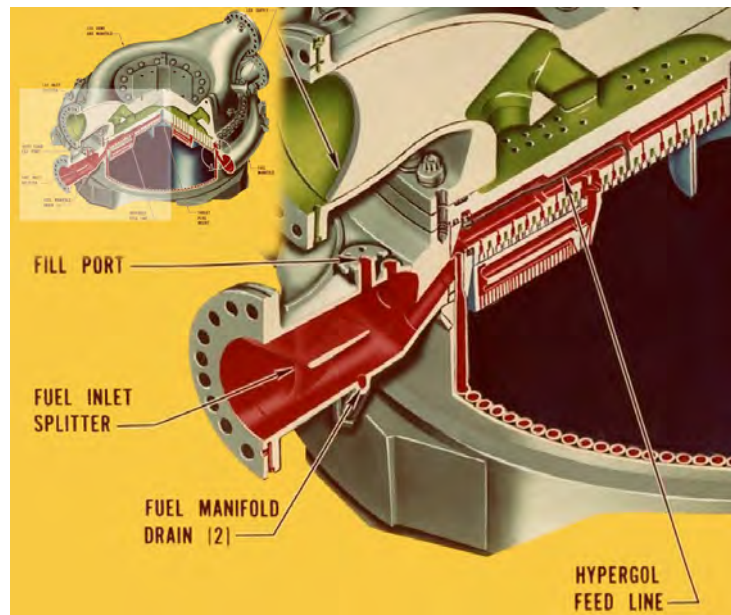
Fig. 1.1: Rocketdyne F1Propellant Manifold Diagram Showing Enlarged Detail of Integrated Hypergolic Igniter (adapted from [1])

Most importantly, due to their high levels of reactivity, all commonly implemented hypergols have the disadvantage of high toxicity and/or carcinogenicity. Additionally hypergolic propellants present objective hazards like detonability or corrosiveness and require special material handeling considerations that drive up operating costs. In addition, in the case of leading slug type, hypergolic ignition provides only a single ignition event. For systems requiring restart capability, additional tanks, feedlines and valves are required to handle and deliver the igniter reactants.

Pyrotechnic Ignition

As shown in Figure 1.2, pyrotechnic igniters are essentially small solid motor fuel grains. Pyrotechnic ignitors are the mostly commonly used method for hybrid rocket systems due to simplicity and reliability. Because pyrotechnics are premixed solid oxidizer and fuel combinations, no fluid feed lines are required. Pyrotechnics are typically initiated electrically using an electronic match or squib, which is itself a small self-contained pyrotechnic with a resistive bridge wire embedded in a heat sensitive reactant.

Special handling procedures for pyrotechnic igniters are required due to the same considerations applicable to solid motors and likewise are susceptible to HERO [6] considerations. Nearly all pyrotechnic igniters are single use and cannot be restarted. A limited number of exceptions to this rule exist which have been proposed or tested experimentally [3,10], though these carry low TRL. Most importantly, employing pyrotechnic ignitors serves to defeat "inherently safe" properties of hybrid systems.
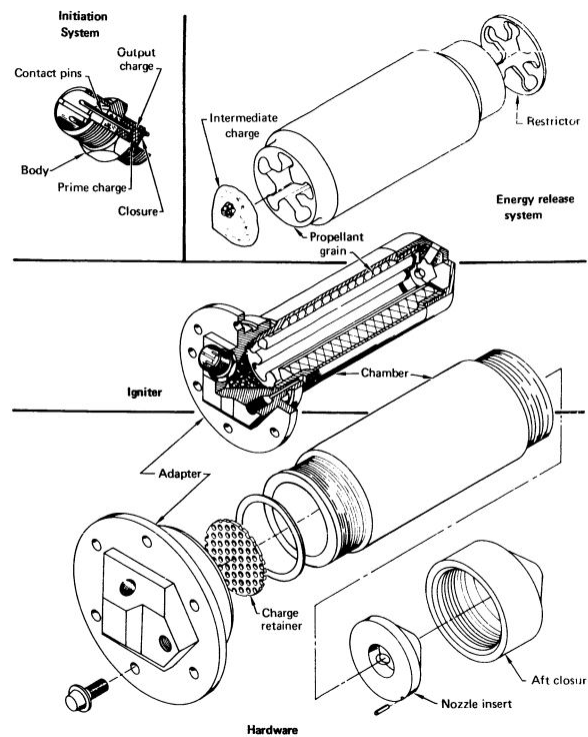

Fig. 1.2: Pyrotechnic Igniter (adapted from [2])

1.5.3 Augmented Spark Ignition

Augmented spark ignition, systems such as that shown in Figure 1.3, are essentially liquid bi-propellant engines with flow rates low enough to allow for direct spark initiation within a separate small igniter combustion chamber. Combustion of the igniter reactants then builds the necessary power release level to ensure reliable and timely ignition of the main propellant. Precedent exists for using high voltage electrostatic arc type ignition sources to the light the main engine propellants [4], though these are typically restricted to very small engines such as reaction control system thrusters. Commonly, main propellants are diverted into this augmented spark or torch igniter, though distinct dedicated ignition propellants may be used, especially in the case of hybrid motors where dual liquid propellants are unavailable.

Augmented spark igniters have been successfully implemented with a high degree of reliability in a number of systems such as the SSME and J2 liquid engines [4], however these ignition systems carry the disadvantages inherent to liquid bi-propellants, including increased complexity and the potential for hard start. For bipropellant liquid systems, an augmented spark igniter provides the advantage of operating with the main propellants, avoiding complications that arise from carrying additional distinct igniter reactants, however this advantage is lost in the application to hybrids where at least on additional dedicated liquid reactant is required.

1.5.4 Catalyzed Ignition

For specific propellants, initiation of combustion may be achieved catalytically. Common catalytically ignited propellants include hydrazine, hydrogen peroxide, and to a lesser extend nitrous oxide. Catalytic ignition systems have been widely used with hydrazine monopropellants using iridium coated alumina catalyst. Hydrogen peroxide was researched heavily and a number of suitable catalysts exist, though use of hydrogen peroxide has generally fallen out of favor due to a combination of low performance and difficulty in long term stability while storing the propellant [14].

Promising research is ongoing in the catalytic decomposition of nitrous oxide [28].
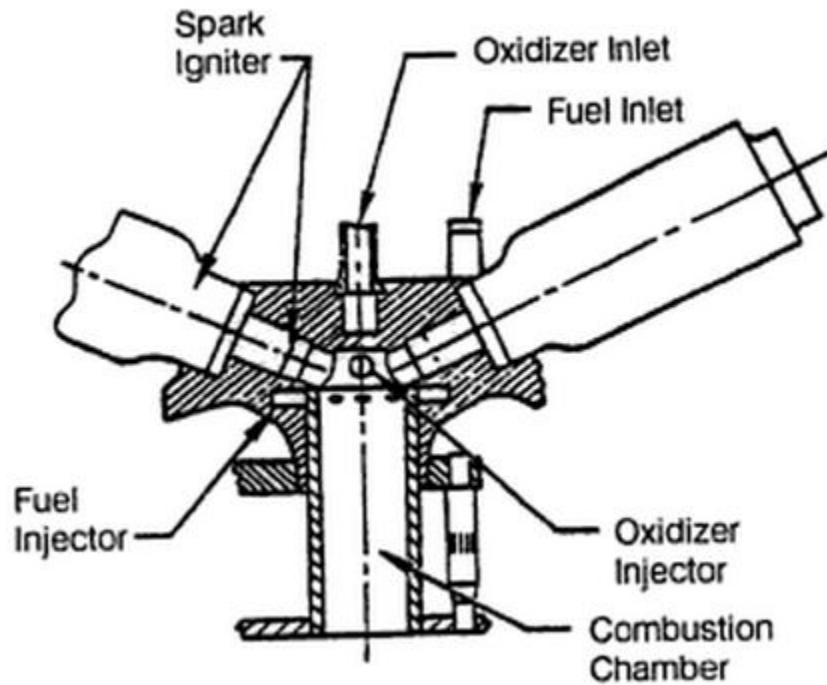
Fig. 1.3: Augmented Spark Igniter (adapted from [3])

Such systems hold the potential for hybrid motor ignition without additional reactants as well as nontoxic monopropellant systems. Technical difficulties with these systems remain however, primary among which is maintaining the integrity of the catalyst during operation. Additionally, catalyst bed preheating is typically necessary placing additional constraints on the system by requiring large power and current supplies and introducing an inherent system response latency.

1.5.5 Plasma Torch Ignition

A plasma torch igniter uses electrical energy to directly heat a gas to form a high temperature plasma flow. Studies have been performed exploring the potential for this type of igniter to be used in both rocket and air breathing engines [29]. In typical operation a plasma torch igniter uses either spark gap discharge or electrically generated radio frequency induction to heat a gas that is then discharged into the combustion chamber. The flowing gas may be one of the propellants such as hydrogen or methane.

Thus the system may be designed to use only the main propellants without the need for separate reactants.

A distinct disadvantage of plasma torch igniters is the need for high electrical power input. Because the energy to heat the gas is provided electrically without any augmentation from chemical reactions large currents and power levels are required.

1.5.6 Single Stage vs. Multi-Stage Ignition

A key consideration in the design of an ignition system is the orderly and timely way in which combustion is initiated in the main propellant flow. This consideration is especially important for liquid rockets where introducing excessive unburned propellant into the chamber may result in catastrophic hard start. For this reason it is desirable to cause uniform, rapid ignition of the entire propellant flow timed precisely with the introduction of flow into the chamber. With ignition methods that begin with electrical initiation it is typically not feasible to provide the required energy directly, and thus multi-stage 'bootstrapping' concepts are employed.

In a multi-stage igniter the source of initiation energy is used to ignite a small amount of reactive material, either flow diverted from the main propellant lines or reactive material stored separately. The hot gas flow from this initial reaction is then channeled, often through a sonic throat, to ignite either the main flow or an even larger quantity of igniter reactants. Thus energy is added to the flow in a controlled manner and at no point is there the risk of collecting significant quantities of uncombusted oxidizer and fuel mixture. Additionally the igniter may run for some time before main propellant flow is introduced thus allowing for instantaneous ignition of propellants in the chamber.

Multi-stage igniters have the advantage of turning small initiation energies at the point of initial reaction into large ignition energies within the main chamber. However, multistage ignition systems typically increase overall system complexity when compared to direct initiation. For example the RSRM ignition method used as part of the Space Shuttle system involved a 4 stage ignition sequence [30]. Thermal management for

the igniter chamber and throat must be considered along with methods for passing hot gas into the chamber. For most large scale rocket motors however, aside from hypergolic ignition systems, multi-stage ignition involving at least one step between initiation and main chamber ignition has historically been the only practical method to assure controlled ignition of the main flow.
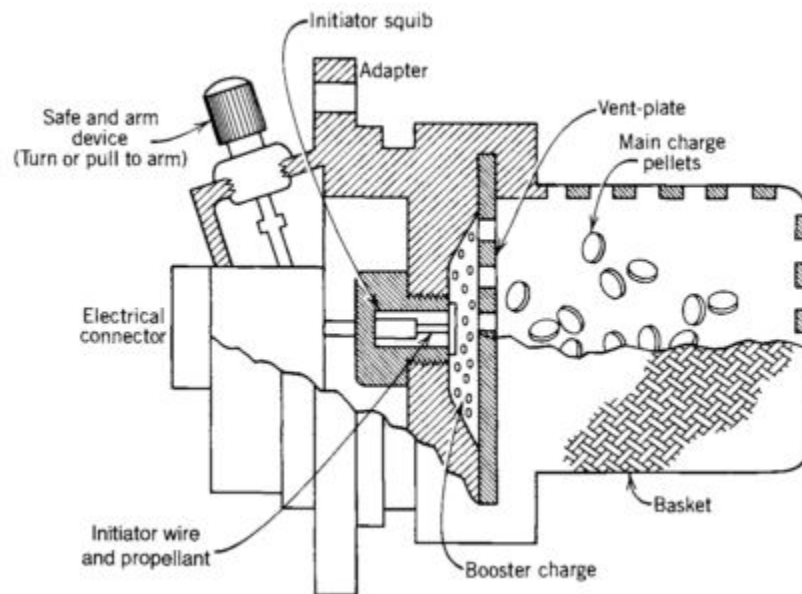
Fig. 1.4: Multi-Stage Pyrotechnic Igniter (adapted from [4])

1.6 Selection of an Ignition System for Hybrid Motors

As was discussed previously, the ignition of hybrid motors poses unique challenges. The ignition system must provide enough energy to pyrolyze the solid fuel as well as have enough residual energy to initiate combustion. Additionally, designing restartable hybrid propulsion systems has posed significant challenges, notwithstanding that restartablility is commonly presented as a primary advantage of these systems. Though the motor itself may typically be shut off and restarted with relative ease, the difficulty arises in the design of the igniter. Selection of an ignition method for hybrid motors poses unique challenges with the current ignition solution space lacking. Table 1.1 tabulates the specific disadvantages of state of the art ignition systems for use in hybrid motors.

Table 1.1: Hybrid Motor State of the Art Ignition Systems Disadvantages

Type	Disadvantages for hybrids
Pyrotechnics	Negates some safety advantages; Typically only single ignition capability
Hypergol	Negates safety by carrying toxic reactants with explosive potential; Significant increase in complexity due to required second fluid feed system
Augmented spark	At least one additional reactant required; Significant increase in complexity due to required second fluid feed system; Potential for hard-start and chamber rupture
Plasma torch	High electrical power draw; Physically large external power unit (EPU)
Catalyst bed	Viable solution for H2O2 oxidized motors, though low TRL for N2O catalyst systems; Continuing technical challenges with catalyst degradation in N20 systems; May require large power draw for catalyst bed preheating; H2O2 not truly a "green" propellant

1.7 Background on Electrical Breakdown

The concept presented here overcomes the disadvantages of current state of the art ignition systems by directly initiating the combustion of the solid fuel and fluid oxidizer using a low energy electric spark. The fundamental principle upon which the electrostatic arc ignition concept is based is the high voltage breakdown the insulating medium between high voltage electrodes. When a sufficiently strong voltage is applied across an insulator, electrons are pulled free from the material resulting in an electron avalanche referred to as electrical breakdown. Once the insulator is subjected to its

electrical breakdown voltage, a relatively conductive hot plasma path forms between the voltage electrodes in an electric arc. Though the natures of the physical mechanisms vary, electric breakdown has been observed in solids, liquids, and gases.

Gaseous electrical breakdown is especially relevant to this research effort. Paschen first observed and characterized the required voltage for electrical breakdown in gasses in what has come to be known as Paschen's law:

$$V_b = \frac{Apd}{ln\,(pd) + b} \tag{1.1}$$

Equation 1.1shows the relationship between breakdown voltage (Vb), and the product of pressure (p) and electrode spacing distance (d). Constants A and b are properties of the specific gas medium. Figure 1.5 shows the breakdown voltage curves as a function of p*d for various gasses.
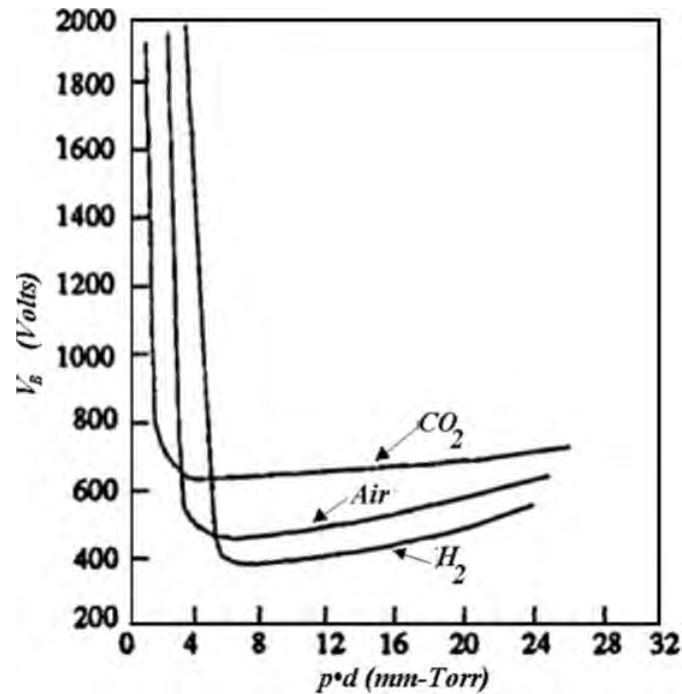

Fig. 1.5: Paschen Curves for Various Gasses

Once electrical breakdown of the insulating material has occurred, a plasma path is formed between the high voltage electrodes, causing a sharp increase in the conductivity

of the current path. If sufficient current is available, the energy dissipated is sufficient to maintain the plasma path and a direct current standing arc may be formed. The voltage and current required to maintain this arc may depend on a number of environmental factors including the free stream gas composition, interactions with electrode shape and the velocity of the gas caused by either free convection or forced flow of the gas across electrodes.

1.8 Application of Electrical Breakdown to the Hybrid Electrostatic Arc Ignition Concept

The concept developed in this effort is substantially different from any previous hybrid ignition systems and is intended to provide a number benefits. These include using only the main propellants as igniter reactants and multiple restart capability.

A number of conditions are required to cause self-sustaining combustion within a hybrid motor. First, as with any chemical propulsion system, the oxidizer and fuel elements must be brought into contact and mixed. In a hybrid propellant combination however, the solid fuel and gaseous or liquid oxidizer will not mix in a way that causes a combustible mixture without a preexisting source of energy to ablate the solid fuel into gaseous byproducts which can mix with the oxidizer. This hybrid attribute, while providing significant safety advantages to the hybrid system, is also the primary source of difficulties in creating hybrid motor igniters which do not involve additional reactants. For hybrid motor ignition, in order to attain mixed reactants, the first condition that must exist is ablation of the solid fuel into fluid components which may then freely mix with the oxidizing fluid.

Second, additional energy must be added to the oxidizer fuel mixture in order to overcome the activation energy and initiate combustion. If the oxidizing element is injected as a liquid part of the energy input required may be to cause a phase change of the liquid to a gases before the reaction can occur. Additionally, some oxidizers such as nitrous oxide also require significant energy input to dissociate the oxidizer molecule into reactive oxidizing components prior to ignition.

Figure 1.6 gives an overview of the direct spark igniter concept where high voltage leads are incorporated directly into the igniter grain. A spark gap is formed between the embedded electrodes. When sufficient voltage is applied, an electrical breakdown occurs through the oxidizer gas in the port across the spark gap. Along the electrical breakdown path a high temperature and relatively conductive plasma is formed. With sufficient constant current input from the high voltage power supply, the resistivity of the plasma dissipates sufficient energy that the very small amount of gas directly in the arc path is maintained at plasma temperatures by simple joule heating, and a pseudo stable circuit is formed through this conductive path. At locations where the arc is in contact with grain surface, heat transferred from the plasma causes ablation of the solid fuel. The gaseous fuel products and oxidizer then mix and, with activation energy provided by the spark plasma, initiate combustion. This combustion causes further ablation of the solid fuel and the reaction progresses until port pressure rises and the hybrid combustion becomes self-sustaining.

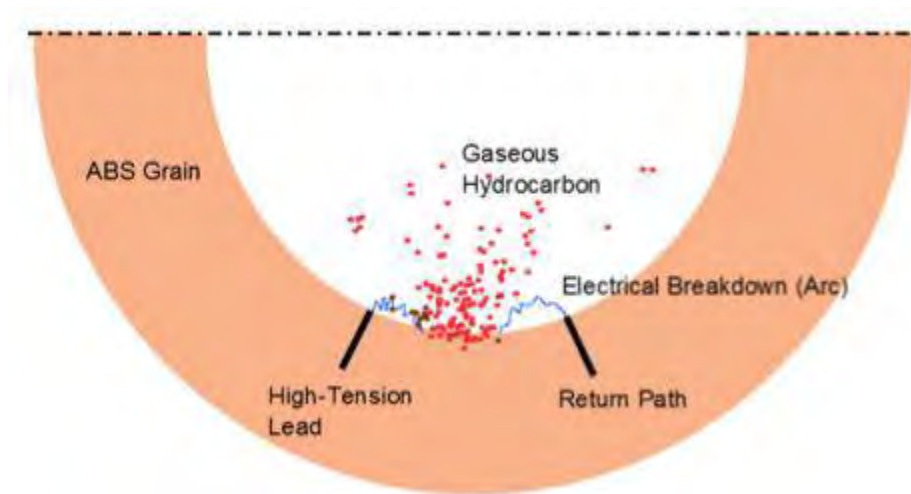Fig. 1.6: Hybrid Electrostatic Arc Ignition Concept

The use of conductive fuel electrodes or a spark which travels along the surface of the grain is key to this concept in order to cause ablation of the solid fuel. Non-ablative metal electrodes such as those used in a traditional spark plug do not place the high temperature plasma of the spark in direct contacts with the fuel surface, but rely on a

gaseous medium already consisting of a combustible mixture. In order to cause ablation, this type of spark gap would need to heat the bulk oxidizer between the spark location and fuel surface to sufficient temperature to decompose the solid fuel. Heating the bulk gas to solid fuel ablation temperatures would require much larger power and total energy inputs than are envisioned for the electrostatic arc ignition concept, essentially creating a traditional arc gas igniter. With the use of ablative electrodes or arcs directed along the fuel surface, the required input energy may be lowered by several orders of magnitude.

For example, Figure 1.7 shows an arc experiment where conductive fuel samples were clamped into metal clips and then subject to voltages sufficient to cause electrical breakdown of the atmospheric air gap separating the electrodes. Figure 1.7A shows an arc where the clips were placed too close, such that the arc formed between the metal clips rather than between the conductive fuel samples. Figure 1.7B shows and arc formed between the fuel samples, which in this case are made from paraffin doped with carbon black. Note the distinctive blue to purple color, typical of an electrical discharge in air, which characterizes the arc between the metal clips. In contrast, the arc formed between the fuel samples shows an orange flame indicating combustion of the gaseous paraffin products and surrounding atmospheric oxygen. The application of this observation to the ignition of the hybrid motor is the fundamental principle which allows very low energy spark discharge ignition.
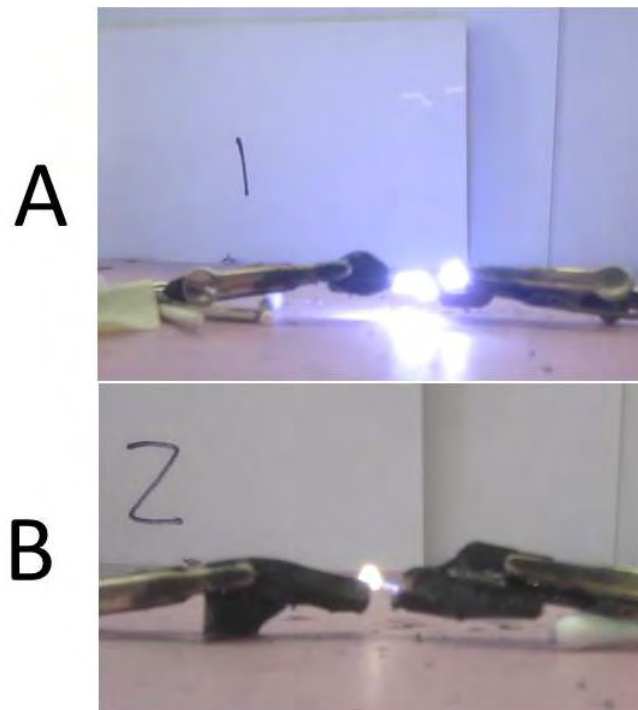
Fig. 1.7: Experiment Showing Differences Arcing Between (A) Metal Electrodes and (B) Conductive Fuel Samples

Chapter 2

Test Apparatus Design and Testing Methods

2.1 Overview of Hybrid Arc Igniter development at USU

This study is part of ongoing research at Utah State University to explore electrostatic arc ignition for hybrid rocket motors. Specifically, the work presented here formed the groundwork for the electrostatic arc ignition concept, that has, since the completion of the experiments presented here, been developed into a highly successful ignition system for 75mm and 98mm experimental hybrid motors at USU. In order to provide context for the key lessons learned during this work, the following discussion gives an overview of the USU hybrid direct spark igniter research to date.

A map of prototype development focused on igniter grain development is given in Figure 2.1. These development prototypes are grouped by test article and show the evolution of the grain design and progression of lessons between this project and other research for electrostatic arc ignition.

Figure 2.1 shows the "evolutionary tree" of the prototypes developed at Utah State. In the initial experiments, the arc discharge path was directed through the core of the oxidizer gas flow. While a number of ignitions were achieved in these tests validating the possibility of electrostatic arc ignition with a low energy spark, ignition reliability was low. Significant difficulties also existed in controlling the spark path, with electrode insulation often fouling from conductive char accumulation, causing the motor to cease to light after 1-3 ignitions.

The research performed during the study presented here built from the base of these early proof of concept tests and solved key problems to create reliable ignition. Key innovations in this work include the development of the surface arcing electrode configuration and the location of the arc in a low flux zone of the precombustion chamber.

As detailed in the results below, running the arc along the gas at the grain surface rather than through the core oxidizer flow removed the need for electrodes separated by a clean insulator, removing problems with fouling. The progression of the fuel grain and electrode configurations tested in this study can again been seen in Figure 2.1.

The igniters in this study achieved reliable ignition with GOX/ABS propellant combinations using a 'strap-on' type external igniter for larger 98mm motors and using voltage levels in range of thousands of volts to initiate arcing. Continuing work has since built on these key lessons learned to develop a surface arcing path directly into the precombustion chamber of larger 75 and 98mm motors at voltages in the range of 200-300 V. This work has led to a highly successful electrostatic arc ignition system for these motors using both gaseous oxygen as well as liquid N2O combined with ABS and HTPB fuels [16] [31].

Test Hardware Design

Data for this study was gathered through testing of three standalone microhybrid motor test articles as well as a dedicated 'strap-on' microhybrid igniter which was integrated into the forward cap of a 98mm hybrid motor case. All versions of the stand-alone motor were built with heavyweight ground test pressure vessels. The use of heavy weight ground test hardware allowed the design to accommodate rapid iteration of grain geometry and spark ignition configuration.

Three versions of the standalone microhybrid were built. Two of these were designed as proof of concept and therefor utilized minimum instrumentation. The third was a fully instrumented test article utilizing existing USU rocket motor test infrastructure. A summary of the hardware used in the various motor firings is shown in Table 2.1.

2.2   Microhybrid Motor Test Article Iteration 1

The first microhybrid motor was constructed as a proof of concept to test the basic feasibility of spark ignition of a solid fuel and gaseous oxidizer. The results for the MH22 test given below were obtained with this test article. The fuel was chosen to

Table 2.1: Motor Hardware Used for Each Test

Test Article Hardware Iteration	Applicable Tests Designations	Test Article Description	Propellants
Microhybrid Iteration 1	MH22	Initial proof of concept microhybrid motor	GOX/FDM ABS Electrodes: HTPB/CB
Microhybrid Iteration 2	MH23, MH24, MH26	Second iteration proof of concept test article with polycarbonate top cap	GOX/Extruded ABS Electrodes: HTPB/CB
Microhybrid Iteration 3	MH30	Fully instrumented microhybrid motor	GOX/Extruded ABS Electrodes: HTPB/CB
Integrated Microhybrid Igniter	MH31, MH32, MH33, MH34, MH35, MH36	Igniter for 98mm N2O/HTPB motor	GOX/Extruded ABS Electrodes: NiChrome

be Acrylonitrile Butadiene Styrene (ABS) based the past research using ABS as hybrid rocket motor fuel at USU and because of ease of manufacture. The primary oxidizer for this study was gaseous oxygen (GOX), though a small number of tests were performed using gaseous nitrous oxide (GN2O).

2.2.1 Prototype System Layout

This motor used an acrylic pressure vessel into which the abs fuel grain was fitted. This pressure vessel was clamped between two aluminum end plates as shown in Figure 2.2. The throat was formed by a drilled hole in the aluminum of the bottom end plate. This was acceptable as burn durations were short and exact control of the chamber pressure was not necessary, removing the need to strictly prevent throat erosion. Gaseous oxidizer was fed into the chamber through a simple square edged orifice drilled into a threaded insert plug assembled into the forward chamber plate.

An ignition spark was provided by a commercial stun gun, Shown in Figure 2.2, using a capacitive type high voltage discharge . The discharge energy of this high voltage

source was limited to not more than 9 Joules per spark. Actual delivered energy per spark was not measured, and delivered energy may have depended on a number of factors including required breakdown voltage between the electrodes and charge state of the stun gun battery.

During operation, the high voltage source caused an electrical breakdown forming a momentary spark through the gaseous oxidizer in the grain port between the consumable electrodes. This action caused vaporization of the electrodes at the point of the spark and added the energy necessary to begin combustion of the fuel and oxidizer. Spark frequency was not independently controllable and varied from approximately 5 to 50 Hz depending on the required breakdown voltage between electrodes. Higher required breakdown voltage resulted in lower spark frequency.

For the proof of concept tests, a simple feed line was constructed using a GOX bottle, a pressure regulator and a solenoid valve as shown in Figure 2.2. Because the intended purpose of this motor was only to prove the concept of electrostatic arc ignition, no instrumentation beyond video recording of the firing and the pressure gauge on the downstream side of the regulator was provided. The motor was secured with clamps to a cart during testing. Oxidizer flow control was provided through a manual switch controlling the solenoid valve. Spark control was provided by manual operation of the commercial stun gun. During testing a two person team operated the spark and valve control manually under the direction of the test controller. This system allowed for rough control of the order of spark vs. oxidizer flow timing during start-up.

The firing procedure was to first purge the chamber with a short GOX flow by opening the GOX valve. This purge was performed before the first test as well as between subsequent tests. Then a countdown was performed and the test operator manually initiated the firing. Successful firings were performed with both the spark actuated first followed by valve actuation as well as vice versa, though typical operation lead spark before oxidizer flow. Because all actuation was performed manually for the proof of concept tests timing varied but typical spark lead was on the order of 1 second.

2.2.2 Microhybrid Iteration 1: Grain development

Grains for this test article were additively manufactured with a MakerBot 3D printer. This is a Fused Deposition Modeling (hot melt) type printer which extrudes a thermoplastic ABS wire to form three dimensional geometry. Grains were printed to final shape including the initial port inner diameter and two radial holes approximately 0.1" in diameter running from OD to ID and placed 180 degrees apart about $\frac{1}{4}$ of the length down the grain as shown in Figure 2.3. The initial grain ID was nominally 0.2" with a circular cross-section. Grain length was 1.2" with a 0.625" OD. The material was a natural color ABS plastic provided in spooled wire form from MakerBot.

Consumable electrodes were cast in place in the radial electrode holes in the grain. The electrodes were formed using a mixture of 5% carbon black in HTPB by weight. This mixture was injected into the radial holes until approximately flush with the ID of the grain port as shown in Figure 2.3. Wires were fed through insulated pass-throughs in the top end plate. These ran along the outer diameter of the grain to each consumable electrode where they were embedded and allowed to cure in place. The arcing path for this electrode configuration passed radially through the core gas flow of the circular port.

As discussed in detail in the results section, char plating on the internal surfaces of the grain after the first burn was observed to cause shorting of the electrodes and prevent motor ignition during initial testing. In an attempt to prevent shorting the surface path between electrodes was increased by creating a grain separated into two pieces by a center slit as shown in Figure 2.4. This grain shape did not eliminate surface arcing and was abandoned after a single test. All subsequent grains used cylindrical port geometries.

2.3 Microhybrid Motor Test Article Iteration 2

As shown in Figure 2.5, a second iteration of the microhybrid motor was build where in the top aluminum end plate was replaced with a polycarbonate cap in order to eliminate a short path to ground through the motor pressure vessel structure. The injector remained a screw-in NPT threaded insert with a simple square edged orifice.

Because this test article was again intended primarily to gather qualitative rather than quantitative data, the feed-line and and instrumentation were identical to the Iteration 1 tests.

Three tests, MH23, MH24, and MH26, were performed with this configuration. MH23 used the COTS stun gun power supply; however, for the remaining burns a higher power, variable voltage supply was used. This supply was a commercially available "Jacob's ladder" [32] science demo kit. This supply gave increased control over the spark with an adjustable voltage output though a potentiometer adjustment, however instrumentation to determine the exact output was not available.

MH24 and MH25 used grains with cast in place radial electrodes spaced 180 deg apart as was used in the previous firings. Based on lessons learned from these firings, MH26 used radially opposed electrodes as well as a third cast in electrode spaced 0.30" distance axially from one of the two radial electrodes as shown in Figure 2.6. The first ignition of this motor used the radial electrodes and subsequent ignitions intentionally ran the high voltage arc through along the surface of the grain along the length between the axially spaced electrodes.

The Iteration 2 motor was fired using the same oxidizer feed line setup as iteration 1.

2.4   Microhybrid Motor Test Article Iteration 3

As shown in Figure 2.7, a third iteration was designed and built with the purpose of gathering quantitative data to characterize the ignition requirements and motor performance. This configuration used a similar acrylic pressure vessels bounded between end plates. A graphite nozzle insert was added to the bottom plate to allow for simple throat size interchangeability between tests. For simplicity, the nozzle was designed as a sonic throat only and not include any divergent section.

The top plate was constructed of a three layer assembly with a polycarbonate insulator between two aluminum plates. This feature allowed for a metal interface for the screw in injector element and avoided the top plate being consumed during the burn

while still electrically insulating the top inner surface of the chamber from a ground path. The structural bolts that passed through the top plate were insulated with plastic bushings to insure that the combustion chamber head end and injector remained electrically isolated.

The grains employed in the Iteration 3 test article were machined from commercially available extruded ABS bar stock. As shown in Figure 2.8, these grains employed an axial spark gap of 0.3" that intentionally arced along the surface of the grain in the axial direction. For these grains, the electrodes were NiCrome wire cast into place with epoxy and protruding slightly into the grain port. The high voltage side electrode was connected to the electrically isolated portion of the top plate and the low voltage electrode was connected to the bottom plate. Wire between the electrodes and end plates were routed along channels cut into the OD of the fuel grain that were filled over with epoxy for insulation.

2.4.1 Test Instrumentation

Testing of the Iteration 3 motor was accomplished by modifying an existing test stand, the Mobile Nitrous Oxide Supply and Test Resource (MoNSTeR) cart, within USU's legacy propulsion test cell. The MoNSTeR cart shown schematically in Figures 2.9 and 2.10 provides oxidizer supply and feed line infrastructure, a Data Acquisition and Controls (DACS) system, electrical power, and structural mount point for the rocket motor test article. Available instrumentation included pressure transducers, thermocouples, a single degree of freedom thrust measurement stand, oxidizer venture flow meters, and the ability to read various other analog and digital voltage inputs. The DACS system is built around a National Instruments CDAQ [33] with control and data logging software written in NI Labview.

2.4.2 Test Procedures

Table 2.2 details the measurements taken for each test. Tests sequences were run in a fully automated mode using preplanned sequence timing for controlling valves, data

gathering, and spark commands as shown in the sequence event timing in Table 2.3. Time history plots shown in the results section of this paper contain labels referencing these sequence events.

In order to control and measure the voltage and current delivered to the microhybrid system during ignition a precision high voltage DC power supply replaced the "Jacobs Ladder" demonstration supply. This programmable supply provided controlled voltage and current levels on the output as well as direct measurement of delivered voltage and current. Voltage programming and spark sequence event timing was accomplished through an analog voltage signal from a NI 6009 basic Digital to Analog converter (DAQ) which was in turn controlled by the MoNSTeR cart CDAQ. The supply provided up to 14.5 mA at 10,000 V. Supply operation was such that requested DC voltage output would be supplied by the unit's internal closed loop control until the output current limit was reached. At the current limit, the supply output a constant current, and voltage became dependent on the effective resistance of the load applied to the output connections.

2.5   Integrated 98mm Igniter Test Article

Based on lessons learned from the microhybrid motor series, the design was adapted as a reusable igniter for a larger 98-mm, 800 N thrust hybrid rocket motor.. This test article was used for tests MH32 through MH36. The igniter was sized to act as a "strap on" replacement for the pyrotechnic charges that had been previously used to ignite the motor. This resulted in the system shown in Figure 2.11. The 98mm motor was a commercially available Cesaroni hobby motor case with a custom designed head-end cap. This motor was chosen due to previous experience at USU and existing MoNSTeR car infrastructure to support 98mm motor testing.

Figure 2.12 shows a detailed schematic of the strap-on igniter and its integration with the injector motor cap. Integration of the top cap and igniter assembly with the 98mm motor is shown in Figure 2.13. The strap-on igniter grain was machined from ABS bar stock and utilized an axial surface discharge spark gap based on the Iteration 3 microhybrid motor. An integrated pressure vessel top cap, high voltage pass though, and

31

Table 2.2: Instrumentation Present for Each Test

	MH22	MH23	MH24	MH26	MH30	MH31	MH32	MH33	MH34	MH35	MH36
Igniter Chamber Pressure					x						
98mm Chamber Pressure											x
Feed Pressure	x	x	x	x	x	x	x	x	x	x	x
Ox Massflow					x	x	x	x	x	x	x
Fuel Mass Consumption					x	x	x	x	x	x	
HVPS Voltage					x	x	x	x	x	x	x
HVPS Current					x	x	x	x	x	x	x

Table 2.3: Sequence Event Timing

	Event Time (ms)						
	MH30	MH31	MH32	MH33	MH34	MH35	MH36
Spark On	0	0	0	0	0	0	0
Igniter Valve Valve Open Cmd	500	500	500	500	500*	500	500
98mm Feed Valve Open Cmd	NA	NA	NA	NA	NA	NA	1000
Igniter Valve Close Cmd	1500	1500	1500	1250	1250*	1250	1250
98mm Feed Valve Close Cmd	NA	NA	NA	NA	NA	NA	1000
Spark off	1500	1500	1500	1250	1250	1250	1250

* MH34G valve command delayed 100 ms, Open: 600, Cmd Close: 1350

injector element was formed from Macor machinable ceramic. High voltage was routed through the pass through an upper electrode embedded in the cap. The ceramic cap was clamped in place and RTV sealed to an aluminum retaining bracket that provided structural support and a fluid connection for the igniter oxidizer supply line. This design allowed the high voltage electrode to be electrically isolated from the surrounding aluminum 98mm motor cap as well as from the oxidizer feed line. The injector consisted of a .040" diameter orifice machined directly into the ceramic insulator as shown in the section drawing of Figure 2.12.

Two distinct grain geometry iterations were used in the strap-on igniter testing. The grain initially consisted of a single constant diameter cylindrical port. However, based on lessons learned detailed in the results below, a second iteration with a lager diameter pre-combustion chamber housing the spark gap was designed. A comparison of the igniter grain geometries is shown in Figure 2.14 and a summary of motors and the corresponding grain geometry is shown in Table 2.4. Average grain regression was measured between successive burns by weighing the motor pre- and post-burn and calculating the weight change.

Because of physical constraints imposed by the existing 98mm motor test setup, no fluid connection for igniter chamber pressure measurement was present. Igniter chamber pressure was estimated indirectly from oxidizer flow rate, grain regression measurement, throat size, and predicted combustion product composition.

2.6   Data Analysis Methods

Video was taken of each firing at 30 frames per second. Successful spark could be confirmed both audibly and via the visible glow that penetrated the slightly translucent ceramic insulator or natural ABS fuel grain, depending on the configuration. Video confirmed ignition and helped to estimate the time from initial oxidizer flow to motor ignition.

All data processing and analysis was performed in Matlab computational software. Functions were written for data parsing, handling, display, and analysis. Data sets have been organized and stored using the Matlab '.fig' file type to allow for simplified future reference.

2.6.1   Measurement of Propellant Flow Rates and Igniter Energy Output Rate

In order to estimate the energy delivery rate provided by the igniter during a burn, igniter propellant mass flow rates were measured. Oxidizer mass flow data was gathered using a calibrated venturi flow meter. Upstream and throat pressures were measured and a delta pressure calculated. Fluid inlet temperature was measure using a thermocouple on the venture body. Inlet fluid density was calculated from temperature and pressure. During operation, the venturi pressure drop between the inlet and throat was in the range of 1-1.5 psi. This implies a throat mach number of approximately 0.06 and thus mass flow calculations could be performed accurately assuming incompressible flow.

Total fuel consumed for each test was measured by weighing the motor assembly before and after each burn. Fuel mass flow rate average was then calculated by dividing total fuel consumed by the steady-state burn time estimate. Steady-state burn time was

Table 2.4: Summary of Grain Geometry Used in Each Test

Grain Designation	Applicable Tests	Grain Port Length	Precombustion Chamber Length	Precombustion Diameter	Initial Port Diameter	Spark Gap	Electrode configuration
Microhybrid A	MH22, MH23, MH24	1.7	NA	NA	0.2	0.3	Cast in place HTPB/Carbon Black, Radially opposed
Microhybrid B	MH26	1.7	NA	NA	0.15	0.3	Cast in place HTPB/Carbon Black, Radially opposed for first ignition, Axial surface spark gap for subsequent ignitions
Microhybrid C	MH30	1.7	NA	NA	0.15	0.3	Cast in place HTPB/Carbon Black, Axial surface spark gap
Igniter A	MH32	1.7	NA	NA	0.15	0.3	NiChrome wire to grain ID, Axial surface spark gap
Igniter B	MH33	1.7	NA	NA	0.125	0.3	
Igniter C	MH34, MH35, MH36	1.635	0.325	0.375	0.125	0.3	

estimated based on the time of steady-state oxidizer flow rate.

The igniter power output was calculated as in Equation 2.1 where $\dot{E}_{out}$ is the instantaneous energy output rate of the igniter, $\dot{M}$ is the total reactant flow rate, Cp is the specific heat of the combustion products, T0 is the flame temperature, and Tambient is the initial temperature of the motor.

$$\dot{E}_{out} = \dot{M} * C_p(T_0 - T_{amb}) \tag{2.1}$$

The combustion product constant pressure specific heat (Cp) and combustion temperature (T0) were estimated using NASA's industry standard equilibrium chemistry code, Chemical Equilibrium with Applications (CEA) [34], based on oxidizer to fuel mixture ratio from measured propellant flow rates and igniter.
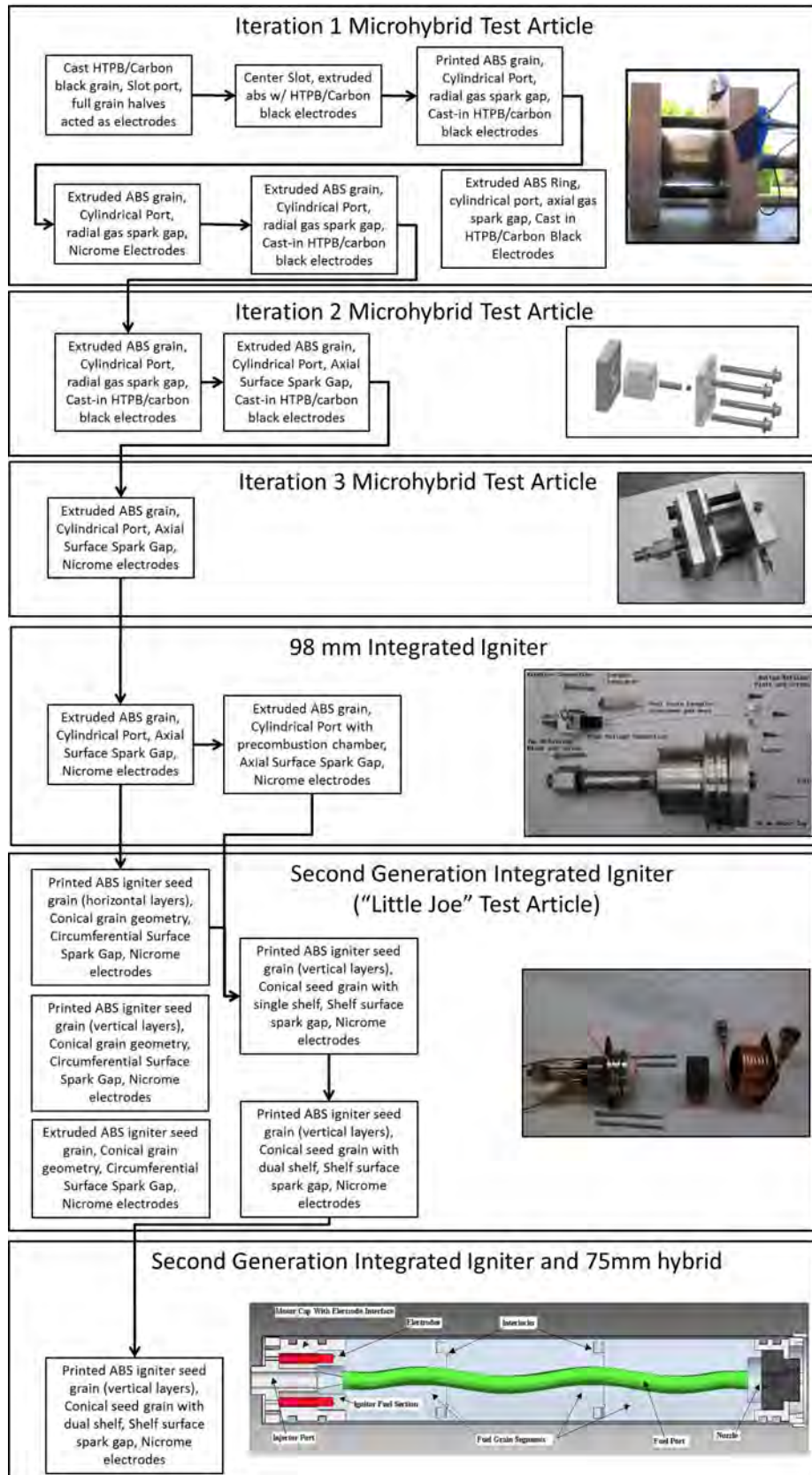
Fig. 2.1: Hybrid Direct Spark Prototype Development Map
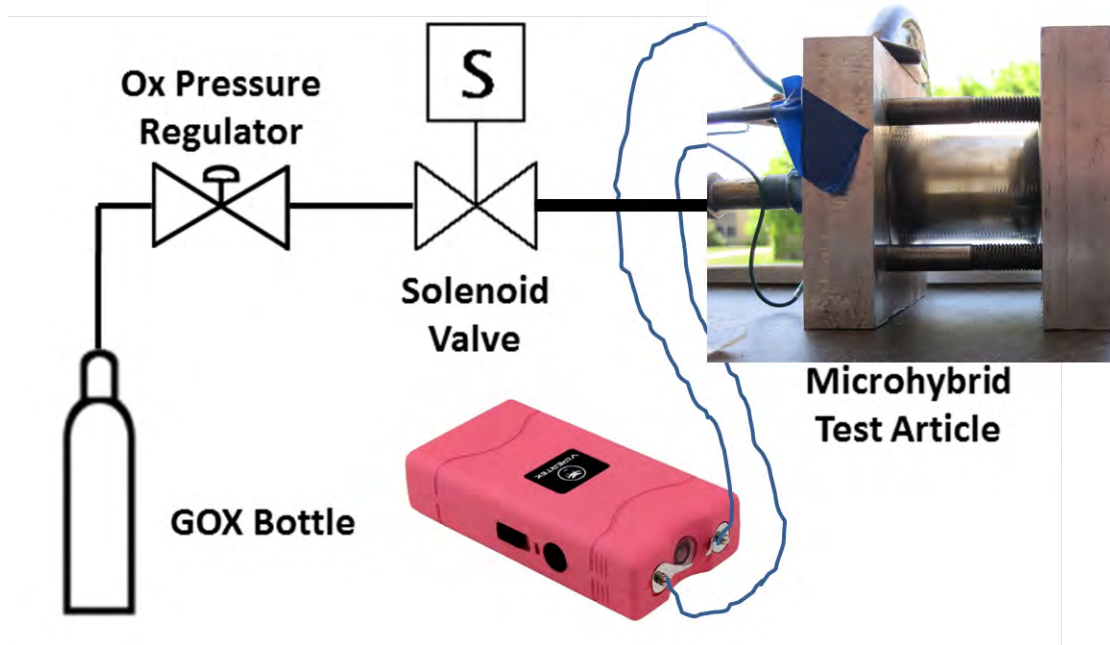
Fig. 2.2: First Microhybrid Feed line and System Setup
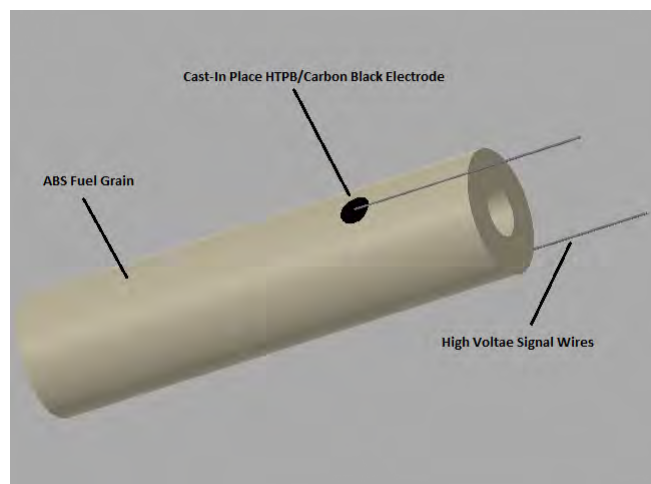
Fig. 2.3: First Microhybrid Electrode Configuration
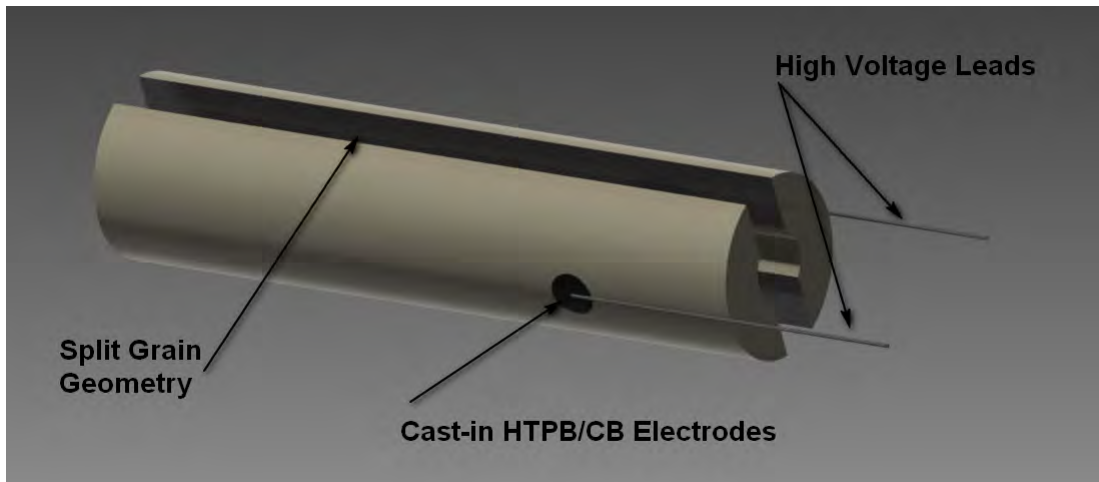
Fig. 2.4: Slit Grain Electrode Configuration
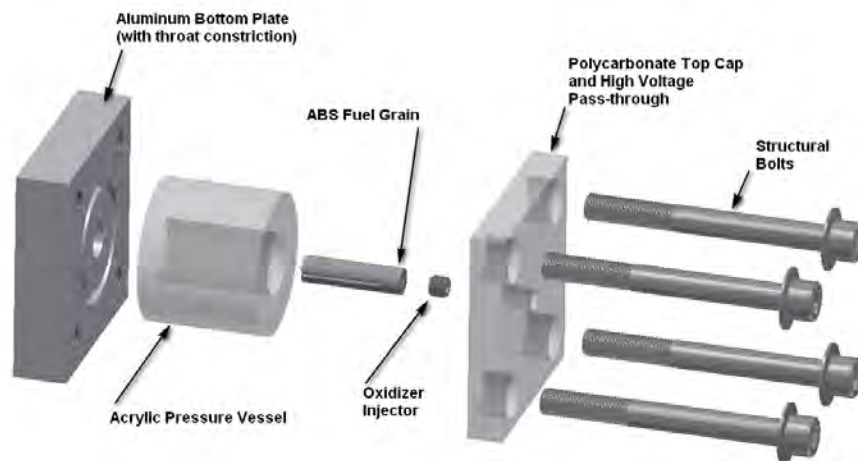
Fig. 2.5: Second Microhybrid Exploded View
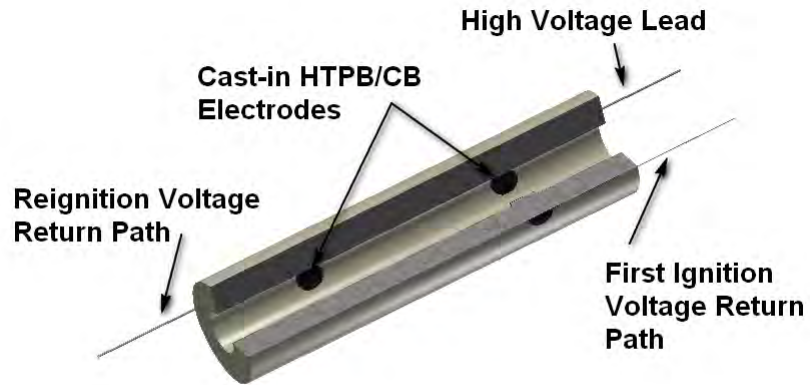
Fig. 2.6: MH26 Electrode Configuration Section View
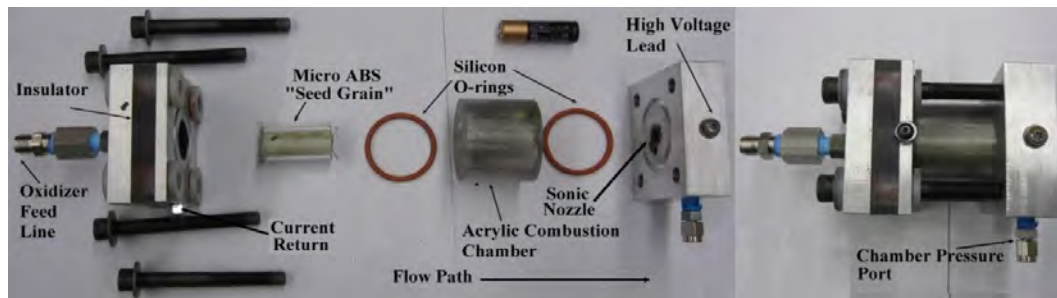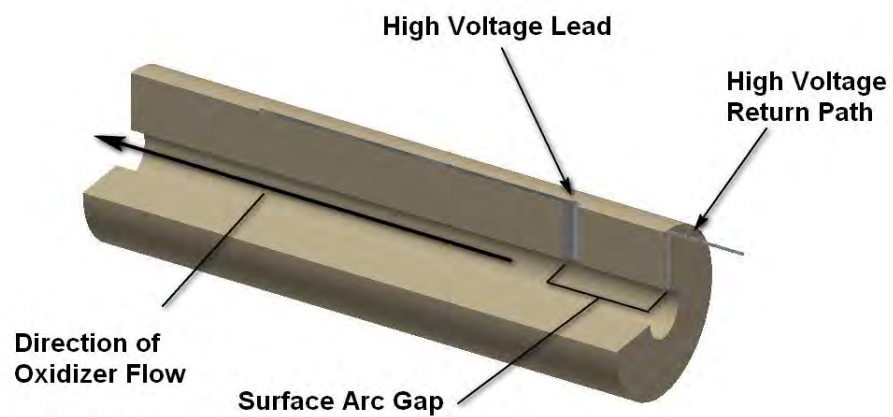

Fig. 2.7: Third Iteration Microhybrid Test Hardware

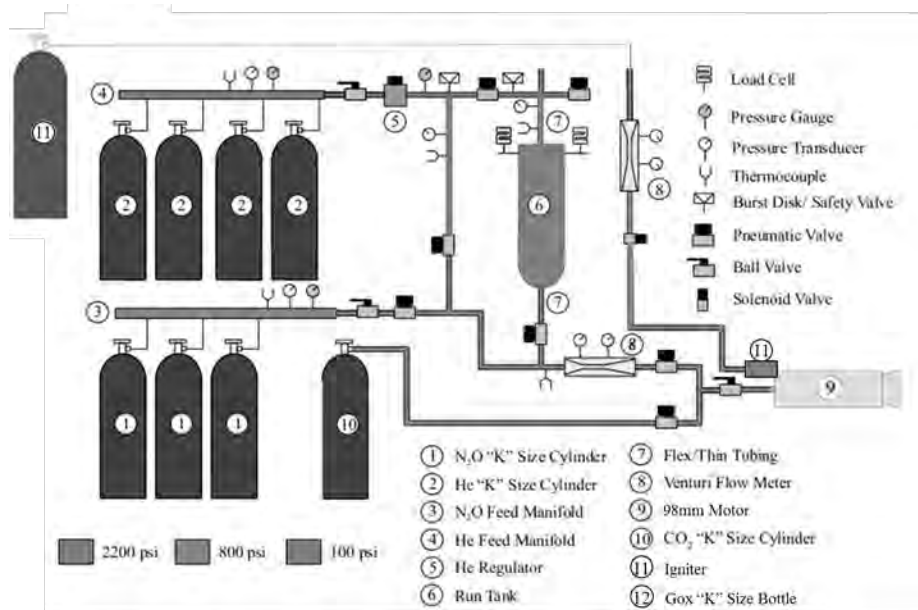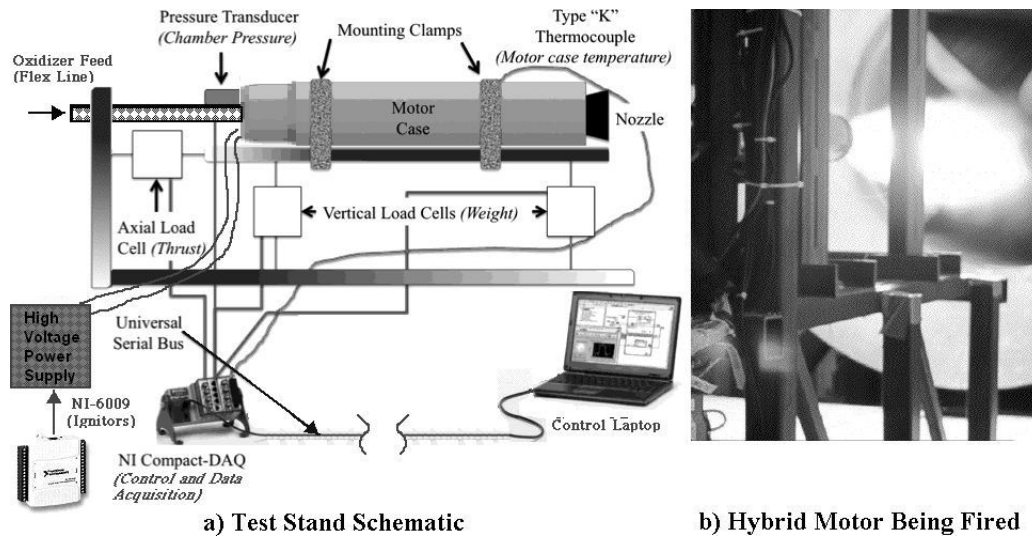Fig. 2.8: MH26 Electrode Configuration Section View

Fig. 2.9: USU MoNSTeR Cart

a) Test Stand Schematic   b) Hybrid Motor Being Fired

Fig. 2.10: USU MoNSTeR Cart
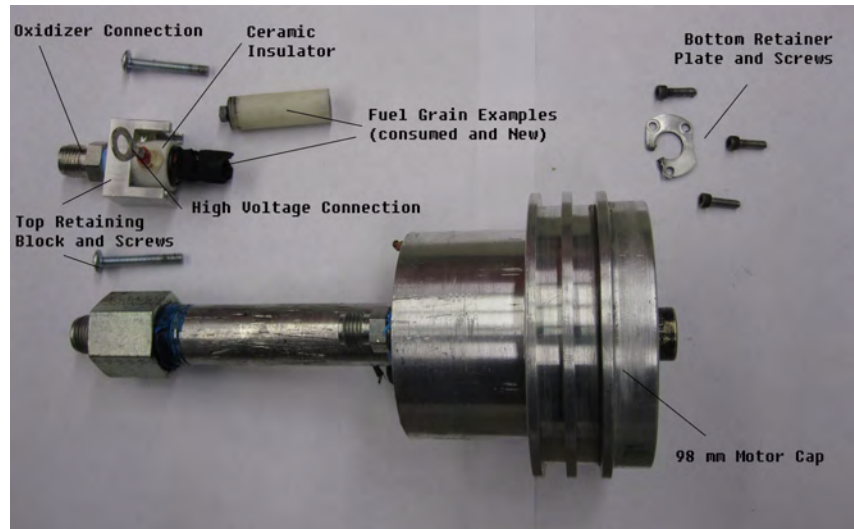
Fig. 2.11: 98mm Igniter Exploded View
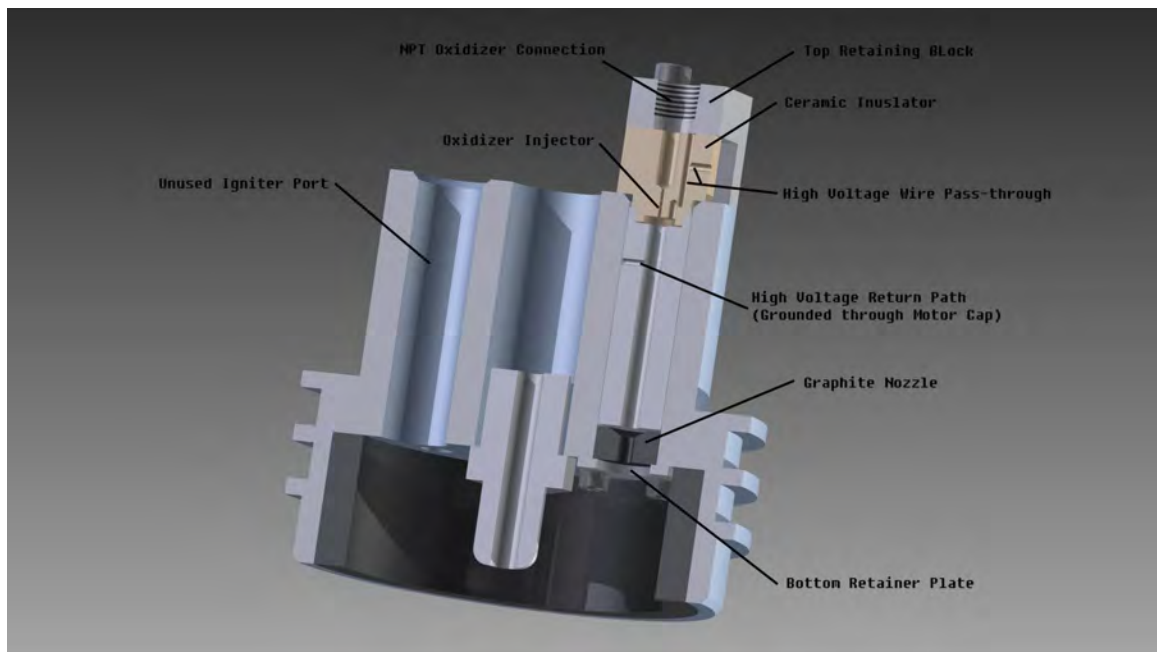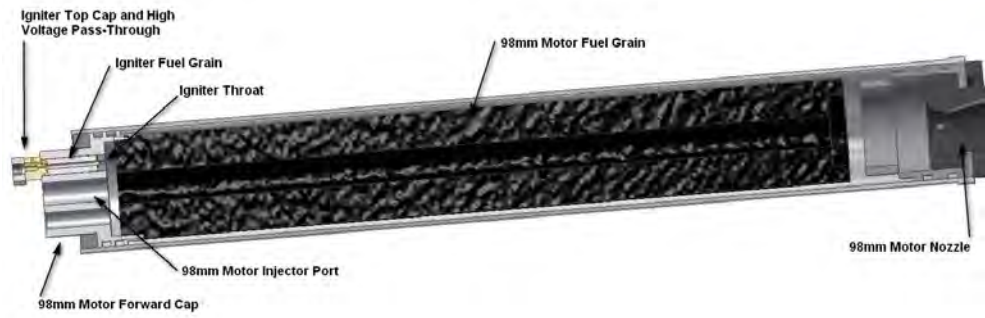

Fig. 2.12: 98mm Igniter Section View

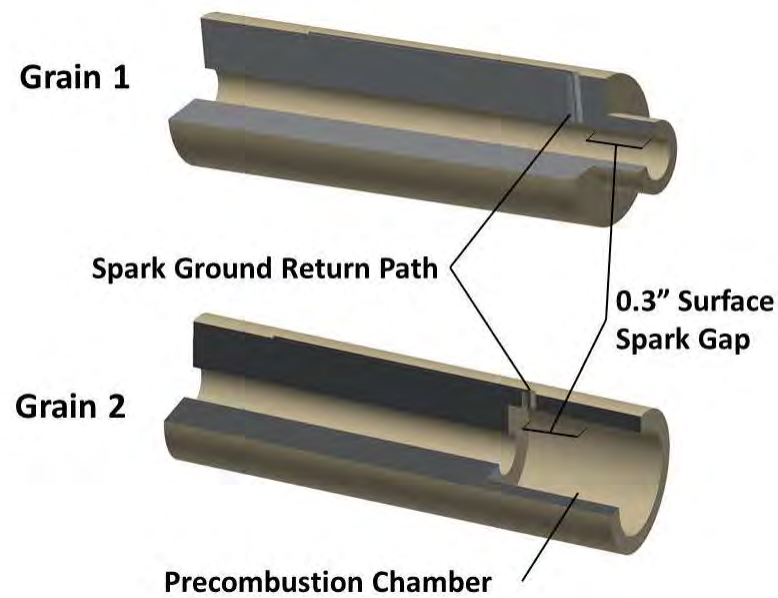Fig. 2.13: 98mm Motor with Electrostatic Arc Igniter

Fig. 2.14: 98mm Igniter Grain Geometries and Electrode Configuration Comparison

Chapter 3

Results and Discussion

Results gathered in this study include both quantitative data as well as qualitative observations. In particular the early proof of concept firings MH22 thorough MH24 were not intended to gather quantitative data and lacked the instrumentation to do so. These firings however produced key observations which guided the designs of later motors and so a discussion of the qualitative results is included here. An overview of the microhybrid test series is shown in Table 3.1.

3.1 MH22 Results and Discussion

The first two ignition attempts of the MH22 motor were unsuccessful, resulting in cold flow of GOX through the motor. On the third attempt and with no notable changes to the setup, ignition was achieved. Multiple successful ignitions followed. Significant smoldering was observed between tests, including some where the GOX purge between firing relit the motor. On these tests the motor was allowed to cool for an addition 30-60 seconds before reattempting the purge and the next test was not performed until the GOX purge could be completed without ignition or smoldering. Testing ended once the motor would not relight. Post-test inspection determined that, while fuel remained, the spark was traveling through soot buildup from the metal electrode to the metal top cap, rather than the intended spark gap across the oxidizer flow path.

The difficulty ignition of this motor was likely due to multiple causes. First, electrical insulation of the high voltage pass was insufficient giving the ever present possibility of unintentional grounding of the high voltage side of the electrode, diverting spark energy away from the initiation point within the motor. This issue was compounded by a sharp increase in the dielectric breakdown strength of the gas through the port once

Table 3.1: Test Objectives and Results Summary

Test Designation	Test Hardware	Test Objective	Results Summary
MH22	Interation 1 Microhybrid	Early proof of concept ignition	Multiple succesful igntions however igntioin not reliable, shorting of spark through char build-up
MH23	Interation 2 Microhybrid	Test of motor with insulating top cap	Multiple ignitions, continued difficulty with shorting through char
MH24	Interation 2 Microhybrid	Test of higher power HVPS	Multiple ignitions, reliable ignition even with continued spark through surface char
MH26	Interation 2 Microhybrid	First test of intentional surface spark gap ignition	Reliable ignition, 27 relights
MH30	Interation 3 Microhybrid	Fully instrumented surface spark gap test article	Reliable ignition, 2 total burns
MH31	Integrated Igniter	Attempt to light with GN2O	No ignitions
MH32	Integrated Igniter	First test of new igniter form factor	Reliable ignition, 3 total burns
MH33	Integrated Igniter	Tested smaller initial grain port size to accommodate more fuel in limited physical volume	No ignitions over 6 attempts
MH34	Integrated Igniter	Test of precombustion chamber spark to avoid spark extinguishment, varied supply pressure (100-525 PSI)	Reliable igntion, 6 total burns
MH35	Integrated Igniter	Repeat of MH34 grain to demonstrate operational readiness for 98mm ignition (small changes to ceramic head), characterize grain regression	Reliable igntion, 5 total burns
MH36	Integrated Igniter	Identical to MH35, first ignition of 98mm motor using microhybrid	Successful ignition/reignition of 98mm motor with 4 sequential firings

flow was initiated. Second, because the power supply was not well controlled and was likely underpowered for the application, successful sparks through the intended gap did not consistently provide enough energy to cause ignition and was the likely cause for the initial failures.

Inability to light the motor after multiple successful ignitions was caused by conductive soot build up along surfaces connecting the spark electrode to ground. After the first ignition the spark was diverted away from the intended path by conductive char buildup. This problem is analogous to the fouling of a spark plug in automotive engines employing spark ignition. In automobiles if the spark plug is not maintained within correct temperature and mixture ratio range, conductive carbon deposits will form on the electrode insulation, creating a path of resistance which is lower than across the intended spark gap. In a hybrid motor, the shutdown transient necessarily passes through a period of fuel rich combustion as the fuel already vaporizing from the surface mixes with the decreasing oxidizer flow as the manifold volume downstream of the feed valve blows down. This forms sooty combustion products which coat the internal surfaces of the motor with relatively conductive, carbon rich products.

3.2 MH23 Results and Discussion

As was discussed previously, in response to the issue of arcing to the grounded metal top cap observed in MH22, the test article was redesigned with a polycarbonate top cap (Microhybrid Iteration 2). Initial attempts to light the motor failed until the feed pressure regulator was turned down from 75 psig to 5 psig. With higher feed pressures, once flow was initiated, the spark was observed to jump the approximately 1.25" air gap between the stun gun electrodes shown in Figure 2.2, rather than across the spark gap within the motor. After the first ignition at 5 psig feed pressure, ignitions were the successfully accomplished at 75 psig feed pressure. However, well before the fuel grain was consumed the motor again failed to ignite. Upon disassemble the grain was sparked again in normal atmosphere revealing that the spark path followed the char layer along the grain and across the polycarbonate cap, grounding to the metal injector element

rather than sparking across the intended spark gap through the port.

A number of important observations resulted from MH23. First, the effective resistance to dielectric breakdown through the spark gap was seen to increase dramatically with the introduction of oxidizer flow. The voltage required to form and arc across the external 1.25" air gap between stun gun electrodes can be approximated using Paschen's law. This results in a calculated value of nearly 150 kV that did not cause an arc across the approximately 0.20" intended spark gap internal to the motor, showing that the required output voltage is prohibitively high for designs attempting to arc through the free stream gas. The solution to lowering the required arcing voltage occurred as a product of the MH24 test described below.

Second, while the use of insulating material in the motor cap had decreased the likelihood of unintentional shorting to ground, controlling the spark path between the electrodes continued to be an issue. This behavior was despite a large increase in length of the surface path to ground. Significant effort was invested into devising designs that would prevent surface arcing and force the spark to travel through the gas in the port. Ideas included inert gas insulation purges, tortuous surface paths between the electrode and nearest ground point, and complex electrode tip shapes.

3.3   MH24 Results and Discussion

The solution to the problem of controlling arc path for reliable ignition came as a result of testing MH24, which again used the Iteration 2 test article. This motor had multiple successful ignitions using same electrode configuration as MH23, but using the more powerful "Jacobs Ladder" power supply. Feed pressure for all firing attempts was set at 75 psig. Initial firing attempts, performed at the low end of the output voltage range, did not lite. Through incrementally increasing the output voltage level with successive attempts, a minimum output voltage setting for successful ignition was established for the initial ignition. Through the same process, a minimum voltage level for ignition was determined for successive firings. Minimum voltage level for successful ignition was found to be higher for the first ignition compared to successive firings. Since instrumentation

to measure the output voltage level did not exist, only relative measurements were taken based on the position of the output voltage control potentiometer.

It is likely that MH24 suffered the same spark path diversion as MH23, however the success of MH24 can likely be attributed to the more powerful Jacobs Ladder supply vaporizing the polycarbonate in the cap as the spark ran along the char deposits to the metal injector. With the increased power supply input the cap became essentially part of the motor fuel and initiated combustion.

This result prompted a rethinking of the problem. Rather than attempting to avoid surface arcing, a solution was devised to intentionally arc between electrodes along the surface of the grain. Electrodes placed axially rather than radially opposed across the grain port ensured that the path of least resistance was always along the surface. This design gave the added benefit of having fuel in contact with the hot spark along the entire length of the spark rather than just at the ends, increasing the potential amount of fuel that was vaporized into the oxidizer flow. Additionally the spark was optimally placed to add heat directly at the interface between oxidizer and fuel, within the gas boundary layer, rather than through the oxidizer free stream.

3.4 MH26 Results and Discussion

MH26 was the final Microhybrid Iteration 2 motor test and was designed to apply lessons learned from MH24 in the redesigned Microhybrid B grain. The electrode placement within the grain was designed to intentionally arc along the surface in the axial direction. The first attempt to ignite the motor was successful using the upper electrodes spanning the fuel grain port at similar voltage settings to those used in MH24. Connections were then routed to drive the spark between from the upper electrode down the length of the grain, intentionally arcing through the char layer on the inner surface of the grain. This design produced successful ignition in every attempt ending with 27 relights of the motor until the fuel grain was consumed. This result validated the surface arcing concept and thus this concept formed the basis of the motor design for subsequent tests.

MH30 Results and Discussion

MH30 began the first of the fully instrumented thruster tests, achieving two ignitions using the Microhybrid Iteration 3 motor with the MoNSTeR cart test infrastructure. Figure3.1a, Figure 3.1b, and Figure 3.1c plot oxidizer feed pressure, oxidizer flow rate, and motor chamber pressure, respectively. Note that for all data plots shown in time, the time axis is zeroed to the command to initiate the spark.

Oxidizer manifold pressure begins to rise at 0.573s for both A and B firings. First indication of oxidizer flow into the chamber, as indicated by chamber pressure rise, occurs at 0.580s. Ignition can be seen to occur at approximately 0.713s and 0.797s after spark command for MH30A and MH30B, respectively. Ignition is preceded by a period of oxidizer cold flow at apparent steady-state for both firings. As would be expected with a small amount of erosion of the graphite throat, steady-state cold flow pressure was slightly higher for firing A at 46 psi compared to 41 psi for firing B.

Figure 3.2a, Figure 3.2b, and Figure 3.2c, plot supply voltage, current, and effective arc path resistance, respectively. Effective arc path resistance was calculated by R=V/I in time. The supply was current limited at approximately 14 mA. For MH30A, effective arc path resistance begins at approximately 65.4 kOhm at spark initiation and decreases nearly to 28KOh at 0.580s just before oxidizer flow initiation. Resistance then increases to approximately 230 kOhm during oxidizer cold flow. After ignition, resistance drops to 32.4 KOhm, decreasing to 8.3 KOhm over the course of the burn. Average Values for effective arc path resistance are shown in Table 3.3.

Arc path resistance begins higher in MH30B at approximately 62 K Ohm. Corresponding to introduction of oxidizer flow into the chamber at 0.580s, the effective resistance spikes to 5100 K Ohm and then oscillates between about 1200 and 3100 K Ohm before falling to 26 K Ohm at the point of ignition around 0.800s. The initial spike in arc path resistance can be attributed to the increase in dielectric strength of the arc path with the increase in fluid velocity and pressure corresponding to initiating oxidizer flow. The sharp decline in resistance at ignition shows an increase in the conductivity

of the port gasses as would be expected with the establishment of the high temperature plasma associated with combustion in the port. This arc path resistance behavior was observed to be typical for all instrumented tests presented in this study and proved consistent enough to be used as an accurate tool for determining the point of flow initiation and ignition for later motors.

Table 3.2: MH30 Burn Parameters

Parameter	MH30A	MH30B
Average Oxidizer Feed Pressure (psia)	530.5	524.2
Average Oxidizer Mass Flow Rate (g/s)	5.64	5.58
Average Fuel Mass Consumption Rate (g/s)	2.48	2.57
Total Fuel Mass Consumption (g)	2.49	2.59
Average Mixture Ratio	2.3	2.2
Average Grain Regression Rate (mm/s)	3.1	1.8

Table 3.3: MH30 High Voltage Supply Parameters

	Pre-Flow Average Resistance (kOhm)	Ignition Peak Resistance (kOhm)	Post-Ignition Average Resistance (kOhm)
MH30A	42.2	227.8	16.1
MH30B	351.8	3492.8	12.0

Power delivered by the high voltage power supply to the MH30 grain for both A and B burns is shown in Figure 3.2d. Integrating this trace in time for the period the supply was active yields a total of 4.2J and 0.5J of total energy delivered by the spark system to the igniter for the A and B firings, respectively. At the point of ignition, the power being delivered to the igniter was approximately 17 W and 10W, respectively.
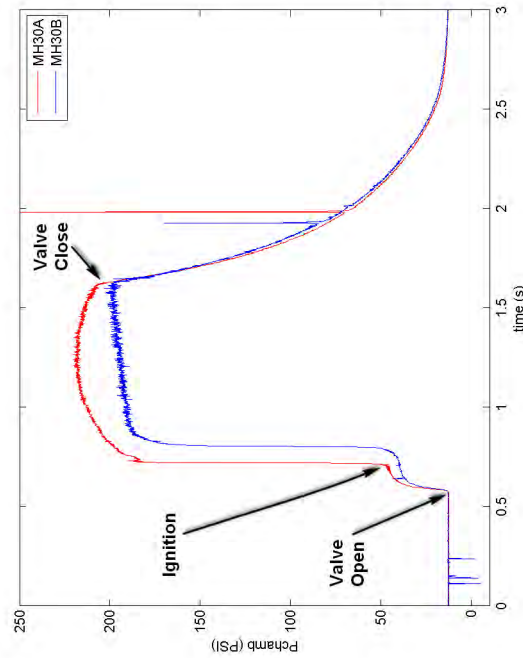
3.5 MH32 Results and Discussion

MH32 began the first of the tests of the strap-on microhybrid ignition system and achieved of 3 successful ignitions. Oxidizer feed pressure and oxidizer mass flow are

50
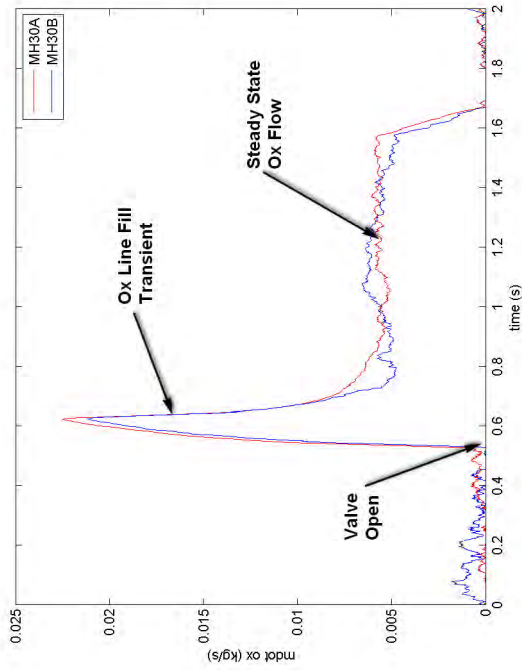
(a) MH30 Oxidizer Feed Pressure
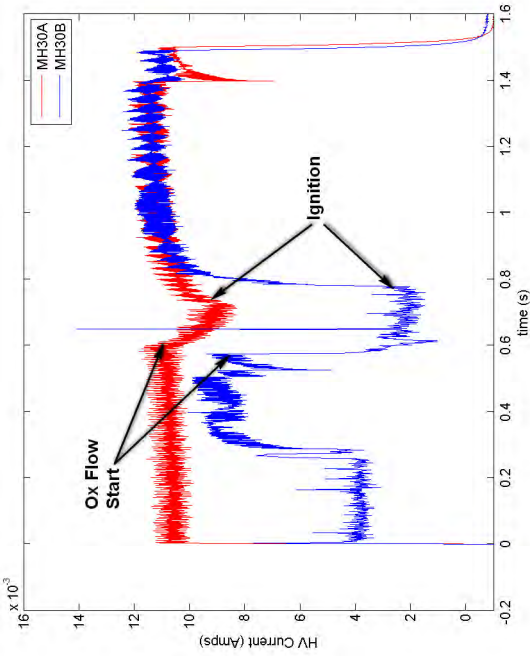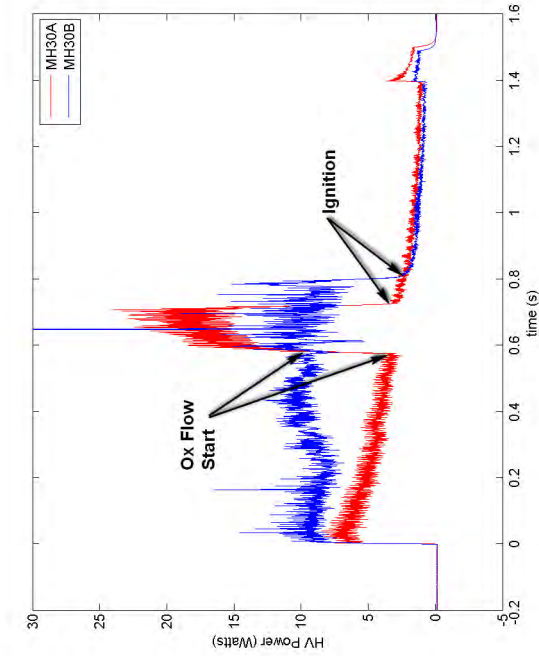
(b) MH30 Oxidizer Mass Flow Rate
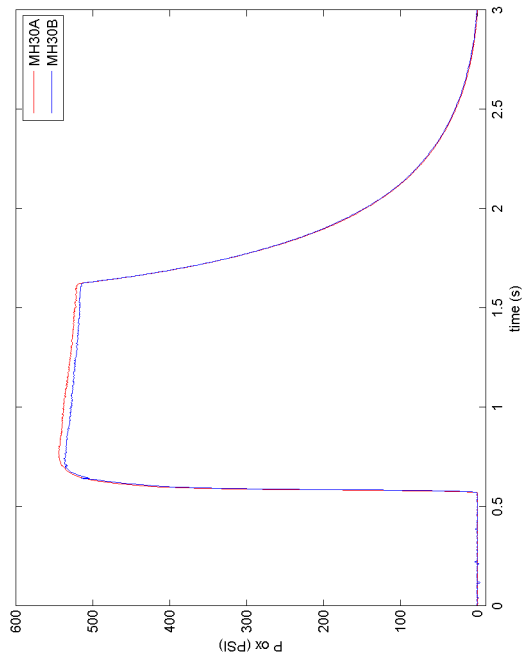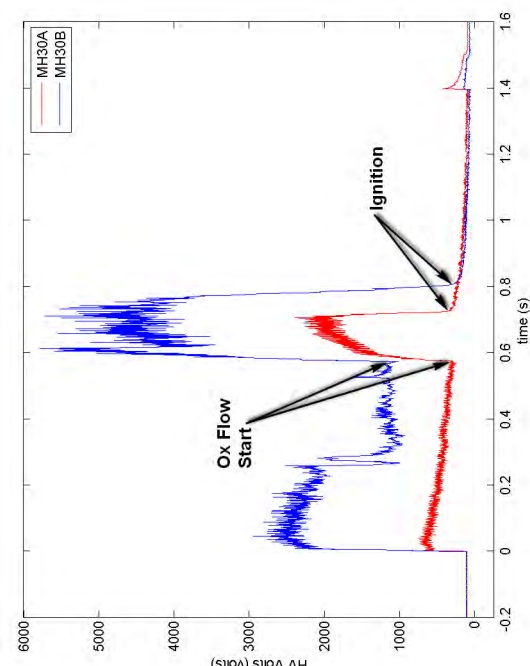
(c) MH30 Chamber Pressure
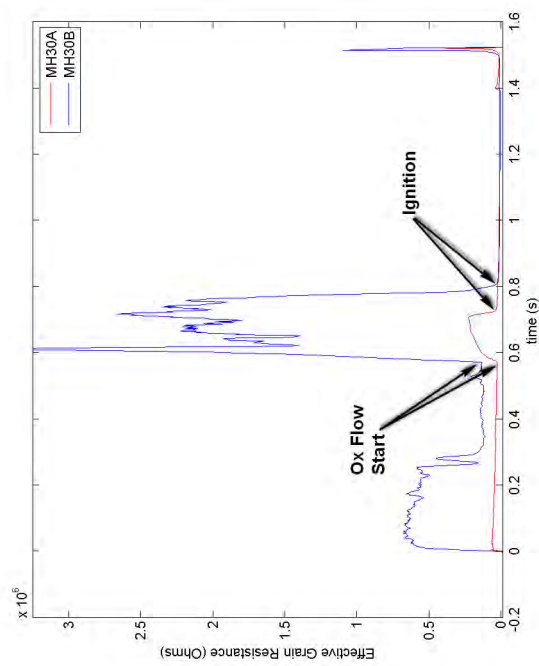
Fig. 3.1: MH30 Microhybrid Firing Data Plots

(a) MH30 HVPS Voltage Output

(b) MH30 HVPS Current Output

(c) MH30 Effective Arc Path Resistance

(d) MH30 HVPS Power Output

Fig. 3.2: MH30 HVPS Data Plots
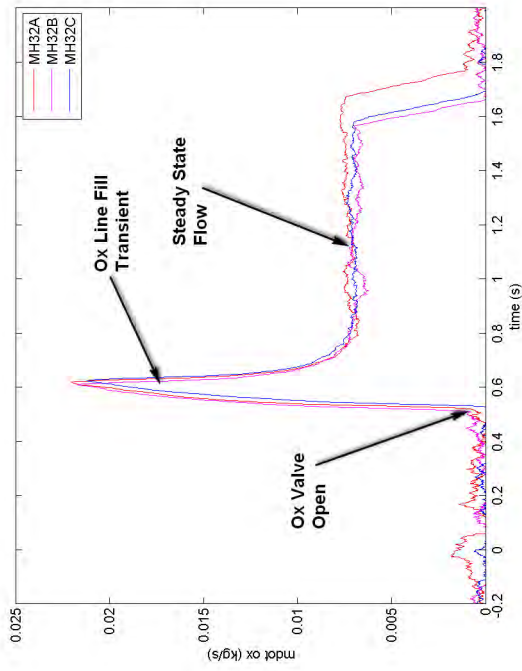
Table 3.4: MH30 Sequence Event Timing

	Event Time (ms)						
	MH30	**MH31**	**MH32**	**MH33**	**MH34**	**MH35**	**MH36**
Spark On	0	0	0	0	0	0	0
Igniter Valve Valve Open Cmd	500	500	500	500	500*	500	500
98mm Feed Valve Open Cmd	NA	NA	NA	NA	NA	NA	1000
Igniter Valve Close Cmd	1500	1500	1500	1250	1250*	1250	1250
98mm Feed Valve Close Cmd	NA	NA	NA	NA	NA	NA	1000
Spark off	1500	1500	1500	1250	1250	1250	1250

* MH34G valve command delayed 100 ms, Open: 600, Cmd Close: 1350

shown in Figure 3.3a and Figure 3.3b, respectively. Oxidizer manifold pressure began to rise at 0.565 s. Steady-state oxidizer flow rates of 7.3, 6.9, and 7.0 g/s were achieved for firings A, B, and C, respectively.

Plots of spark power supply output voltage, output current, and effective arc path resistance for all three firings A, B, and C can be seen in Figure 3.4a, Figure 3.4b, and Figure 3.4c, respectively. The high voltage supply operated in current limited mode during the entirety of all three firings supplying a constant 14.25 mA and causing output voltage to be directly proportional to the effective arc path resistance.
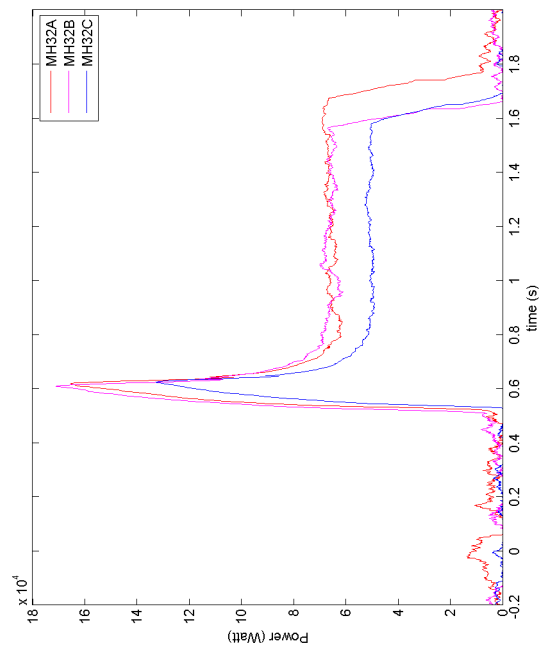
Effective arc path resistance began at an average of 179.5 kOhm in firing A prior to oxidizer flow. When flow was introduced to the chamber effective resistance increased momentarily to 222 kOhm before falling to approximately 20 kOhm. Initial arc path resistance decreased with each firing, with B beginning at 26.5 kOhm and C beginning at 14.9 K Ohm. B exhibited two distinct drops in arc path resistance prior to oxidizer flow at 0.240 and 0.412s. Upon introduction of oxidizer arc path resistance rose in the B firing to 42.5 kOhm before dropping Resistance data suggests that the motor experienced a delay of ignition of approximately 0.10 s after beginning oxidizer flow in the B ignition.
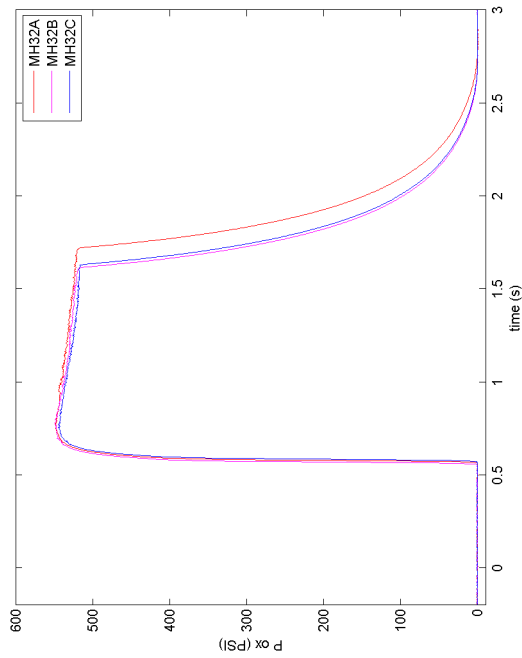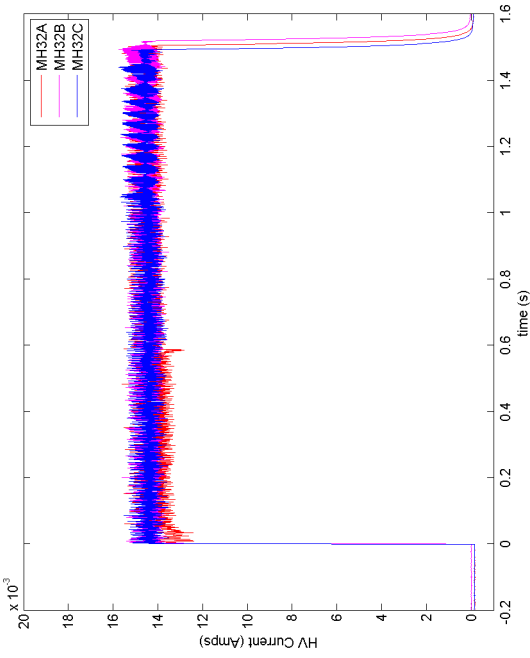
(a) MH32 Oxidizer Feed Pressure

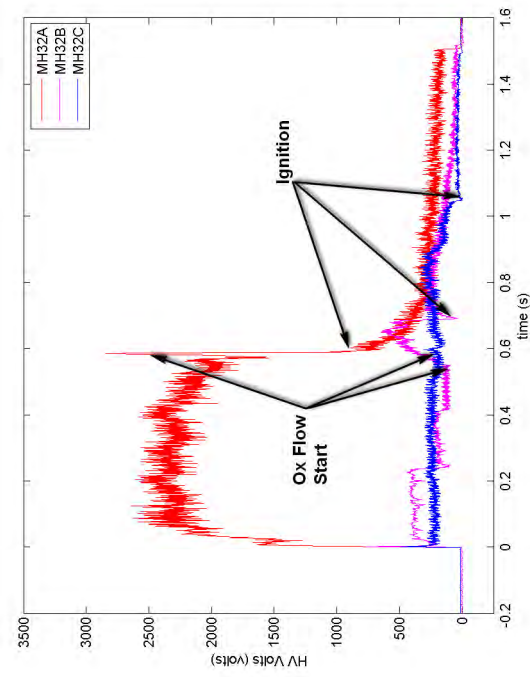(b) MH32 Oxidizer Mass Flow

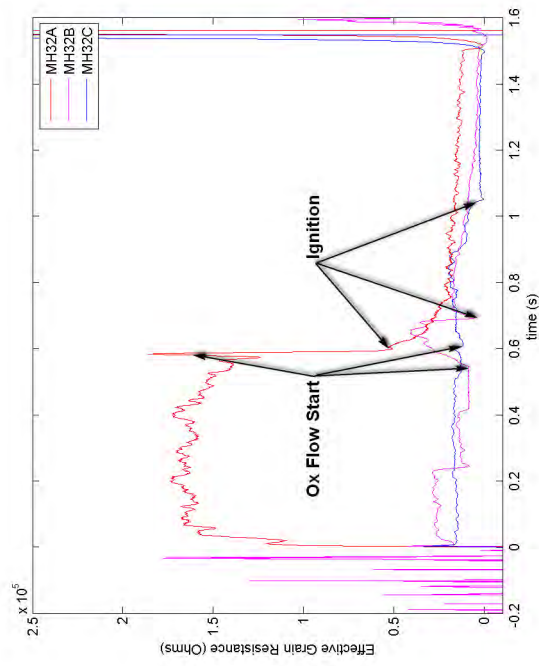(c) MH32 Igniter Energy Output Rate

Fig. 3.3: MH32 Igniter Firing Data Plots

(a) MH32 HV Supply Voltage Output

(b) MH32 HV Supply Current Output

(c) MH32 Effective Arc Path Resistance

Fig. 3.4: MH32 Firing HVPS Data Plots

Approximate energy output rate from the igniter is shown in Figure 3.3c with average steady-state values tabulated in Table 3.5. Note that for the start up transient, oxidizer mass flow rate spikes before falling to a relatively constant steady-state value, causing a corresponding behavior in the calculation of the igniter energy output rate. This is due to filling lines down stream of the flow meter and is therefore an over estimate oxidizer flow rate through the motor. Tabulated values of oxidizer flow rate and igniter energy output were averaged over the steady-state period only.

Table 3.5: MH32 Burn Parameters

	MH32A	MH32B	MH32C
Average Oxidizer Feed Pressure (psia)	533.32	532.57	528.20
Average Oxidizer Mass Flow Rate (g/s)	7.35	6.85	7.05
Average Fuel Mass Consumption Rate (g/s)	1.46	1.52	1.02
Total Fuel Mass Consumption (g)	1.60	1.52	1.03
Average Mixture Ratio	5.05	4.51	6.88
Average Grain Regression Rate (mm/s)	1.18	1.24	0.87

Table 3.6: MH32 High Voltage Supply Parameters

	Pre-Flow Average Resistance (kOhm)	Ignition Peak Resistance (kOhm)	Post-Ignition Average Resistance (kOhm)
MH32A	159.3	185.9	17.2
MH32B	17.6	41.0	11.4
MH32C	15.9	20.1	2.5

3.6 MH33 Results and Discussion

The MH33 test series failed to achieve ignition over 5 attempts (MH33B-F). The test article was identical to that tested in MH32 with the exception of a reduction in

initial igniter fuel grain port size from 0.20" to 0.15" in an attempt to increase the total available ABS fuel under the constraints of the motor cap dimensions. However, in this configuration no complete ignitions were achieved. Comparing flux oxidizer port flux shows that by decreasing the port size the oxidizer flux in the port increased from 3.65 g/cm^2 to 6.23 g/cm^2 between the first burn of MH32 and the ignition attempts on MH33. Time traces of oxidizer mass flow rate can been seen in Figure 3.5, with average mass flow rate tabulated in Table 12.

The high voltage supply data for supply voltage, supply current, supply power output and effective arc path resistance are shown in Figure 3.6a, Figure 3.6b, Figure 3.6c, and Figure 3.6d respectively. Effective resistance averages before initiation of oxidizer flow are shown in Table 13. These do not show notable differences when compared to MH32. After initiation of flow the average resistances also appear similar to MH32; however the characteristic decrease in arc path resistance showing ignition does not occur, with the exception of firing attempts D and E. These tests showed a drop in resistance late in the oxidizer flow period suggesting possible momentary ignition or the establishment of a 'char bridge' along the spark path. Averages of the effective arc path resistance during were calculated and these data are tabulated in Table 3.8.

The high voltage supply current traces show that the supply ran at a nearly constant 14.5 mA. This is consistent with the maximum current the supply is rated to output and shows that it was running in current limited mode. Supply voltage output was then directly proportional to the resistance of the grain surface between the electrodes.

Table 3.7: MH33 Burn Parameters Summary

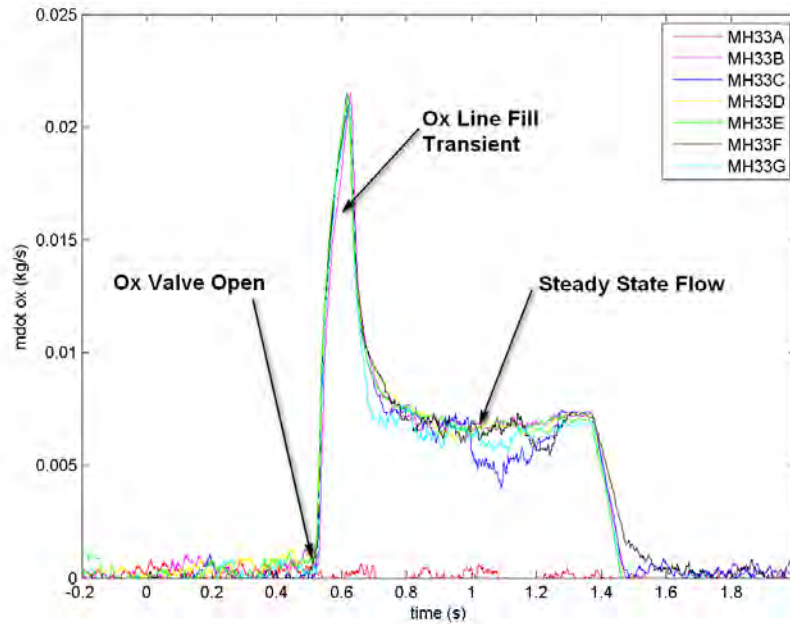|	MH33B	MH33C	MH33D	MH33E	MH33F
Average Oxidizer Feed Pressure (psia)	542	537	538	536	531
Average Oxidizer Mass Flow Rate (g/s)	6.90	6.37	6.81	6.90	6.65

Fig. 3.5: MH33 Oxidizer Mass Flow Rate

## 3.7 MH34 Results and Discussion

Based on the unsuccessful results of MH33, the grain geometry was redesigned with the spark gap located in a precombustion chamber with a larger port diameter. This modification placed the spark in a lower flux location, and MH34 achieved 100% successful ignition with 6 successive firings. Oxidizer mass flow for each firing is shown in Figure 3.7a. Average mass flow along with calculated values for mass flux at the spark location are tabulated in Table 3.9. For these test supply pressure was varied between 100 psi and 525 psi. Figure 3.7b plots the feed pressure time history.

The high voltage supply voltage, current, power output and effective arc path resistance are plotted in Figure 3.8a, Figure 3.8b, Figure 3.8c, and Figure 3.8d, respectively. Table 3.10 presents a summary of arc path resistance. Table 3.11 shows the timing of arc path resistance drops for each of the MH34 ignitions. A trend of faster ignition in motor with lower precombustion chamber flux is evident in the data.
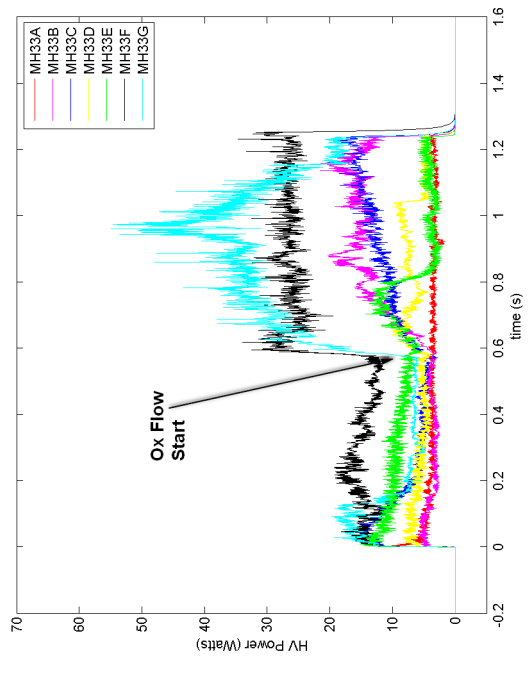
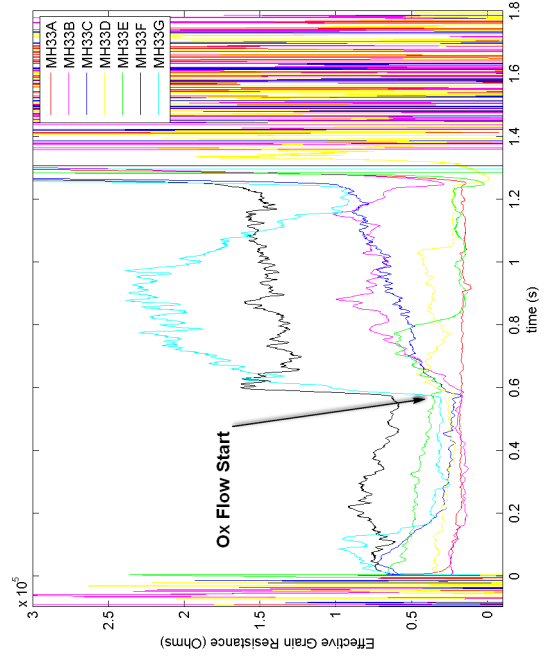Approximate energy output rate from the igniter is shown in Figure 3.7c.
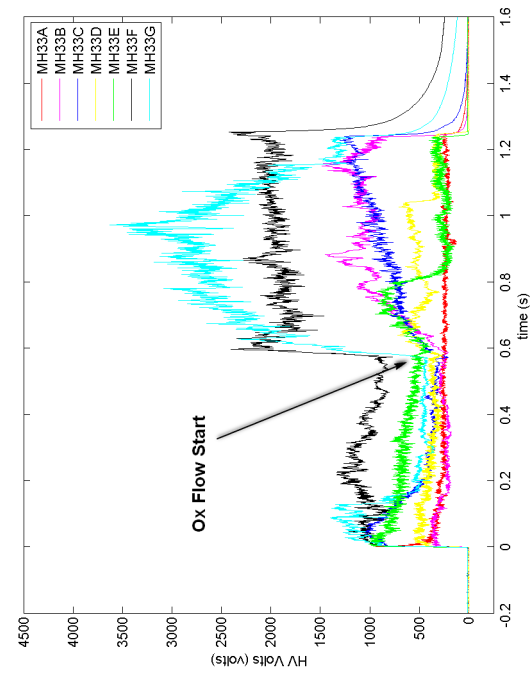
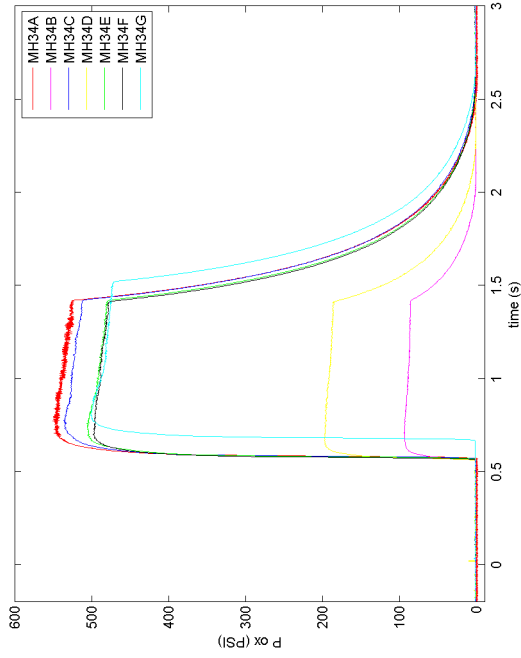(a) MH33 HV Supply Voltage Output
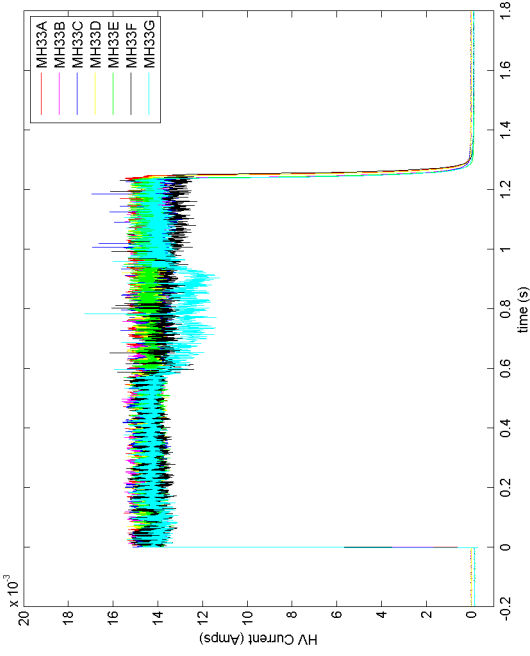
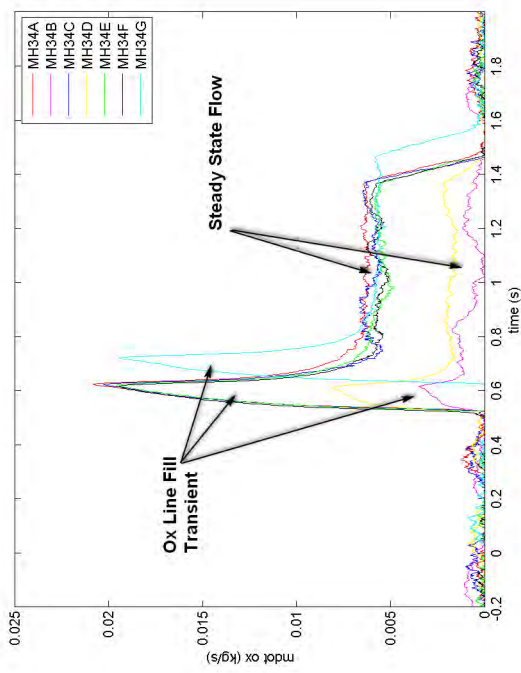(b) MH33 HV Supply Current Output

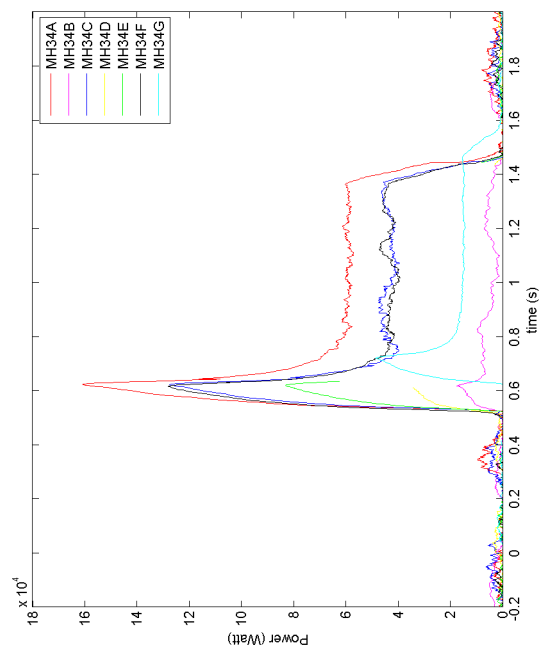(c) MH33 HV Supply Power Output

(d) MH33 Effective Arc Path Resistance

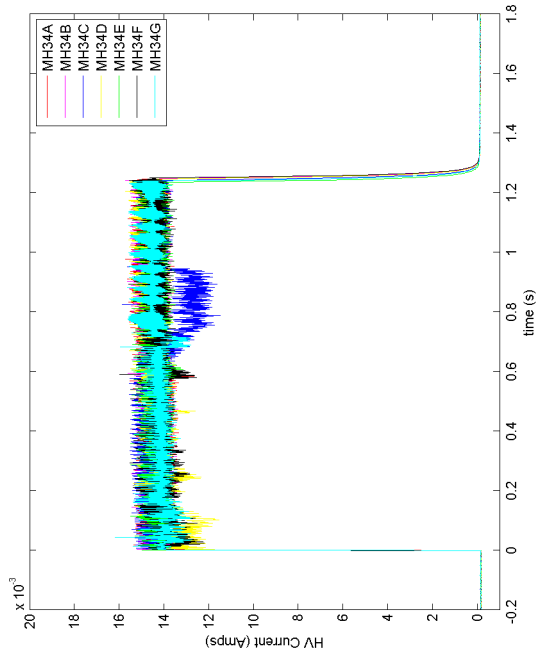Fig. 3.6: MH33 Firing HVPS Data Plots

(a) MH34 Oxidizer Mass Flow Rate

(b) MH34 Oxidizer Feed Pressure

(c) MH34 Igniter Energy Output Rate

Fig. 3.7: MH34 Igniter Firing Data Plots

(a) MH34 HV Supply Voltage Output

(b) MH34 HV Supply Current Output
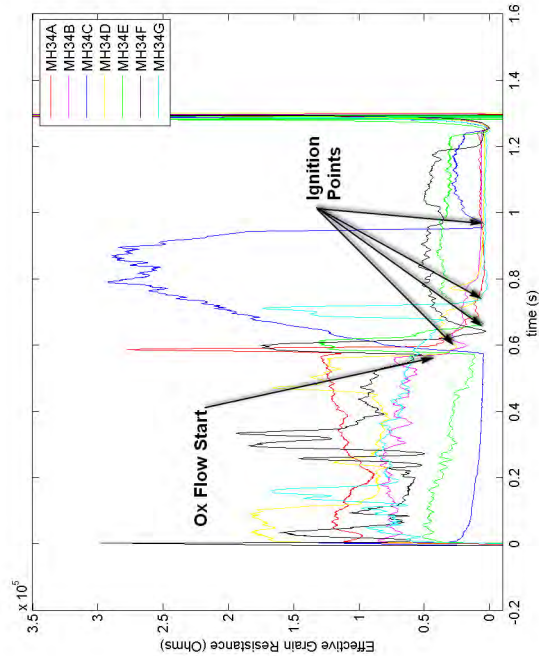
(c) MH34 HV Supply Power Output

(d) MH34 Effective Arc Path Resistance
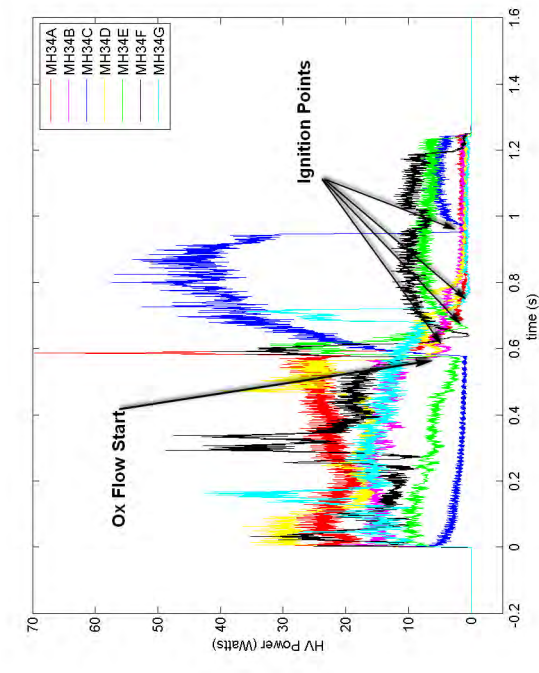
Fig. 3.8: MH34 Firing HVPS Data Plots

Table 3.8: MH33 High Voltage Supply Parameters

	Pre-Flow Average Resistance (kOhm)	Peak Resistance (kOhm)	Post-Ox Flow Average Resistance (kOhm)
MH33B	35.3	115.5	115.5
MH33C	27.6	47.0	22.3
MH33D	46.5	61.3	17.9
MH33E	72.0	189.4	189.4
MH33F	44.8	239.3	188.0

3.8   MH35 Results and Discussion

MH35 used the same spark electrode and fuel grain configuration as MH34 as a readiness demonstration before attempting ignition of the 98mm motor in MH36. This test article achieved 100% ignition success over five burns. Oxidizer mass flow and feed pressure were set to match the highest flow rates from MH34 and are shown in Figure 3.9a and Figure 3.9b respectively. The high voltage supply data for supply voltage, supply current, supply power output and effective arc path resistance are shown in Figure 3.10a, Figure 3.10b, Figure 3.10c, and Figure 3.10d respectively. A summary of arc path resistance values is shown in Table 18. The decrease in initial arc path resistance between firings A and B is notable, and suggests that the pre-firing surface treatment did not represent the electrical properties of a pre-burned grain well.

No significant ignition delay is evident in any of the firings, though burns E and F show faster drop in arc path resistance after introduction of oxidizer suggesting a faster ignition. A summary of ignition times is given in Table 19. Approximate energy output rate from the igniter is shown in Figure 50.

3.9   MH36 Results and Discussion

MH36 was the first test of the strap-on igniter paired with the 98mm diameter hybrid motor. Four sequential tests were performed resulting in four successful ignitions. 98mm motor chamber pressure and thrust are shown in Figure 3.11a and Figure 3.11b, respectively. Igniter mass flow is shown in Figure 3.11c.

Table 3.9: MH34 Burn Parameters

	MH34A	MH34B	MH34C	MH34D	MH34E	MH34F	MH34G
Average Oxidizer Feed Pressure (psia)	535.48	89.00	524.08	190.67	490.43	487.53	482.13
Average Oxidizer Mass Flow Rate (g/s)	6.32	1.08	6.05	1.79	5.59	5.69	5.70
Average Fuel Mass Consumption Rate (g/s)	1.34	0.32	0.89	NA*	NA*	0.89	0.36
Total Fuel Mass Consumption (g)	1.07	0.26	0.71	NA*	NA*	0.72	0.29
Average Mixture Ratio	4.72	3.38	6.82	NA*	NA*	6.40	15.91
Average Grain Regression Rate (mm/s)	1.65	0.32	0.79	NA*	NA*	0.70	0.26

*Weight data not recorded
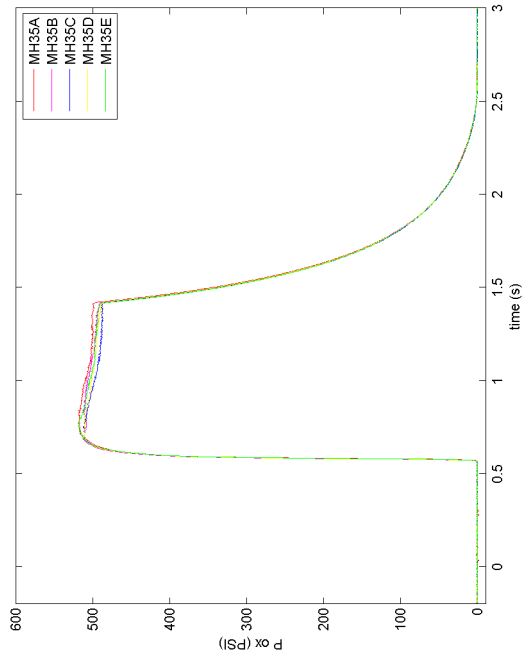
(a) MH35 Oxidizer Mass Flow Rate
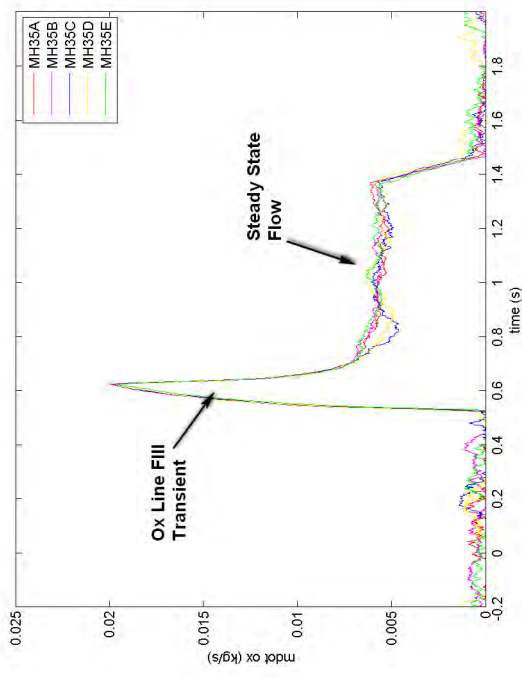
(b) MH35 Oxidizer Feed Pressure
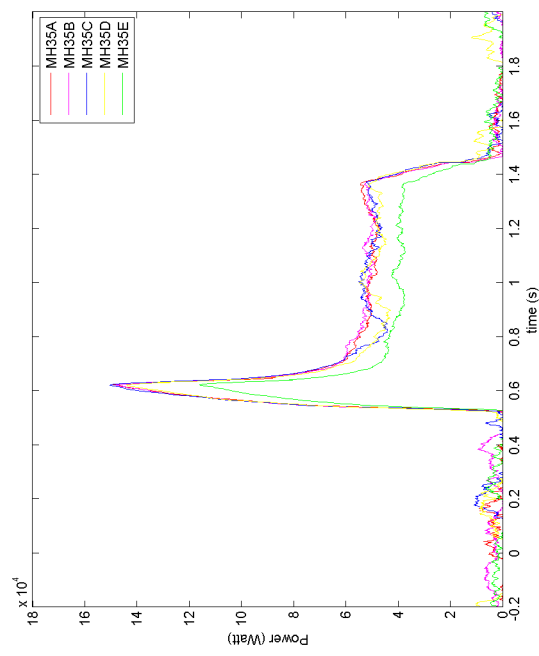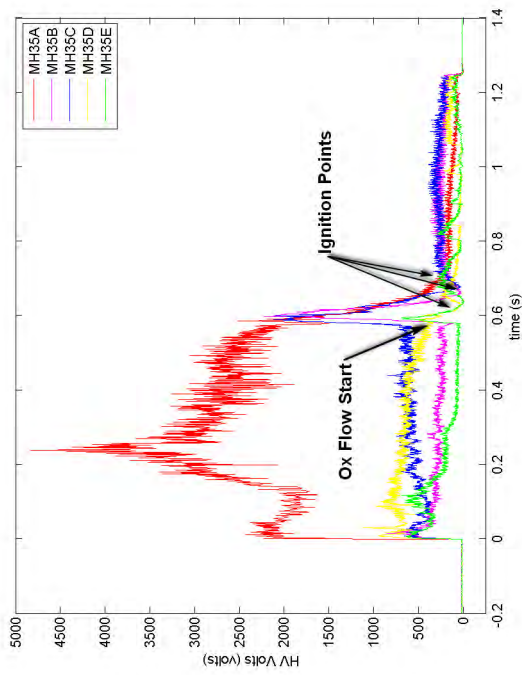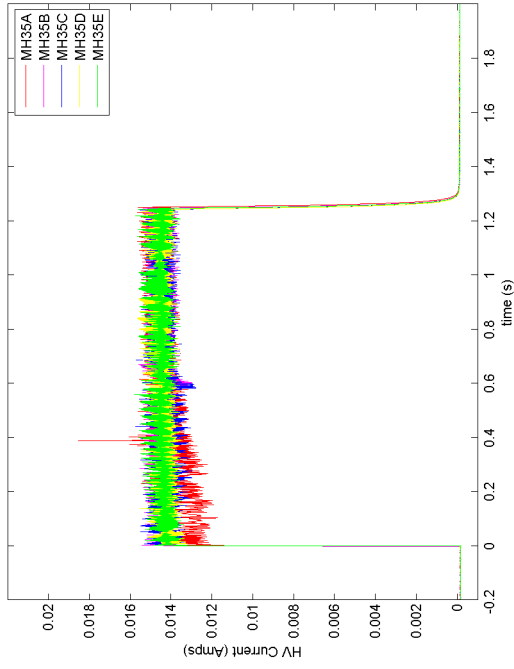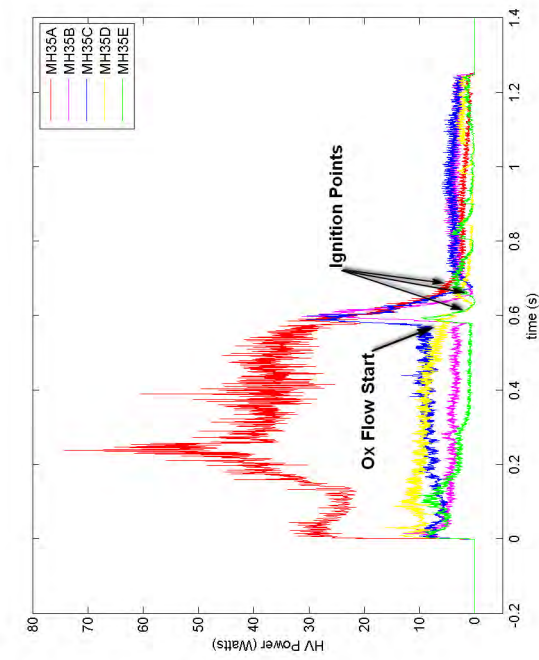

(c) MH35 Igniter Energy Output Rate

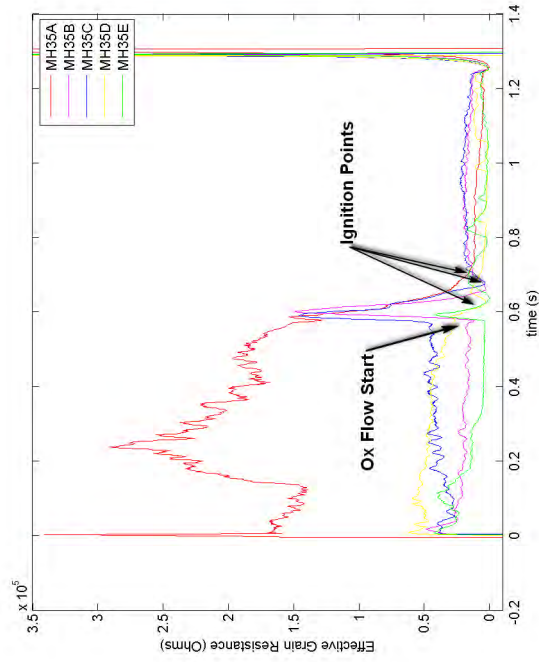Fig. 3.9: MH35 Igniter Firing Data Plots

(a) MH35 HV Supply Voltage Output

(b) MH35 HV Supply Current Output

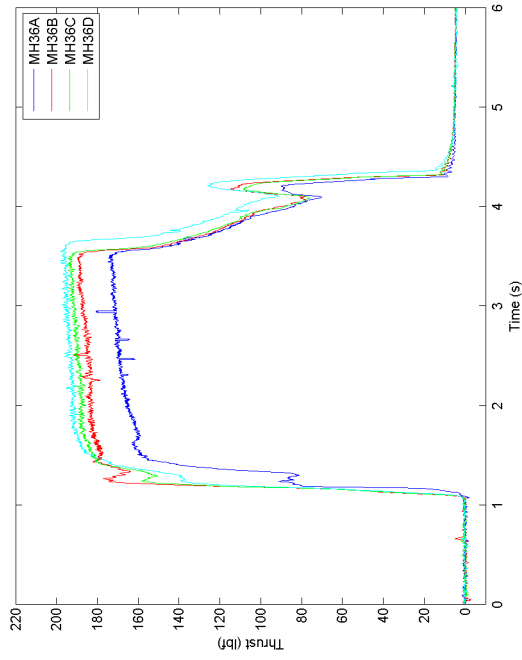(c) MH35 HV Supply Power Output

(d) MH35 Effective Arc Path Resistance

Fig. 3.10: MH35 Firing HVPS Data Plots

Table 3.10: MH34 High Voltage Supply Parameters

	Pre-Flow Average Resistance (kOhm)	Ignition Peak Resistance (kOhm)	Post-Ignition Average Resistance (kOhm)
MH34A	111.8	277.7	9.0
MH34B	72.0	54.8	11.4
MH34C	9.2	292.1	21.5
MH34D	167.8	182.7	11.8
MH34E	32.2	130.7	31.4
MH34F	91.6	175.0	38.8
MH34G	74.3	173.4	3.2

HVPS voltage, current, and power output and effective arc path resistance are plotted in Figure 3.12a, Figure 3.12b, Figure 3.12c, and Figure 3.12d, respectively. MH36A arc path resistance trace shows an ignition delay over 500 ms. This delay correlated well with the delay of the main motor ignition seen in the start-up chamber pressure trace in Figure 3.11a.

MH36 igniter energy output rate traces are shown in Figure 3.11d. A drop in output energy is apparent for MH36D as a result of the lower oxidizer mass-flux. This lower mass-flux is most likely due to inadvertently setting the igniter oxidizer regulator to a lower setting for the D firing. Because of DACS system constraints, an igniter oxidizer feed line transducer was not included in these tests and therefor determining the exact feed line pressure setting is not possible. This test however confirms that significant margin existed on required vs delivered output energy for the nominal igniter operation.
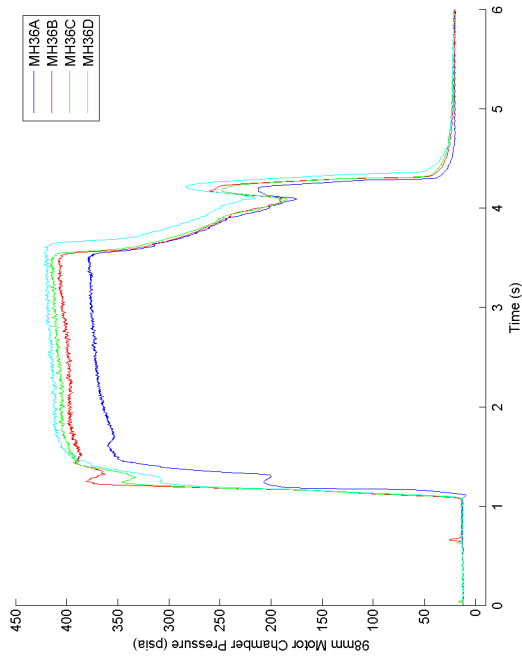
(a) MH36 98mm Motor Chamber Pressure

(b) MH36 98mm Motor Thrust
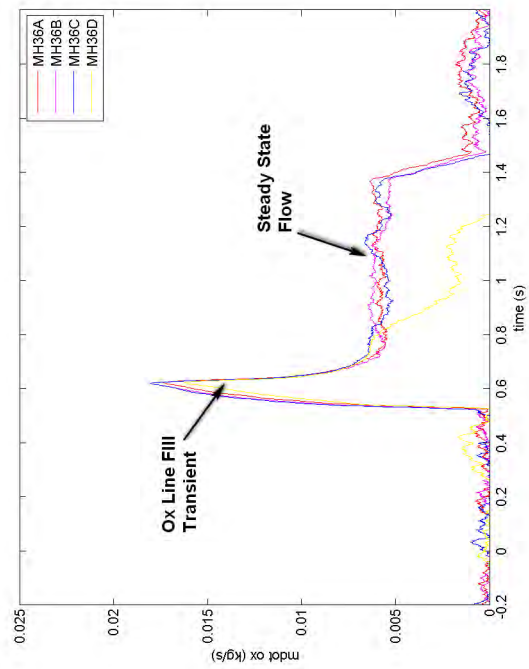
(c) MH36 Igniter Oxidizer Mass Flow Rate

(d) MH36 Igniter Energy Output Rate

Fig. 3.11: MH36 98mm Motor Ignition Data Plots

(a) MH36 HV Supply Voltage Output

(b) MH36 HV Supply Current Output
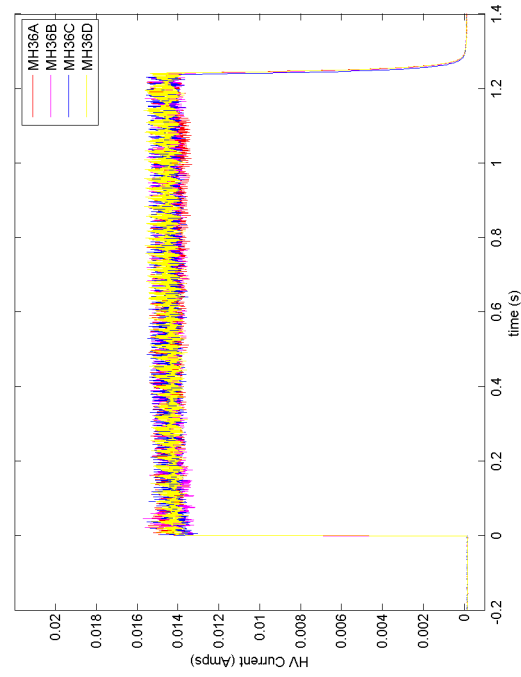
(c) MH36 HV Supply Power Output
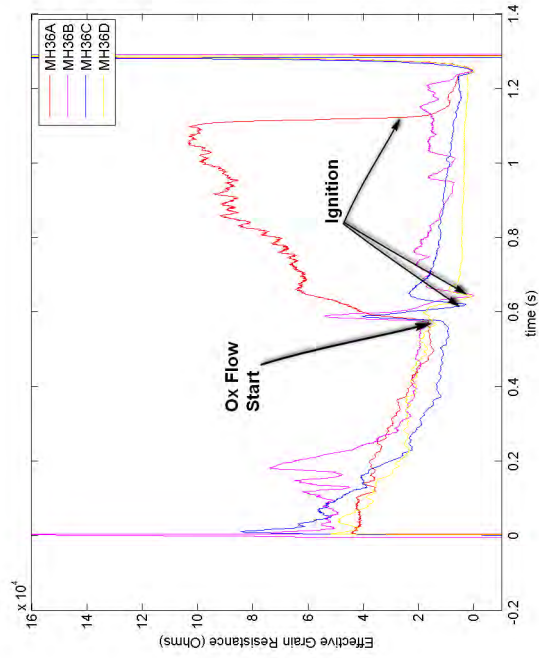
(d) MH36 HV Supply Effective Grain Resistance
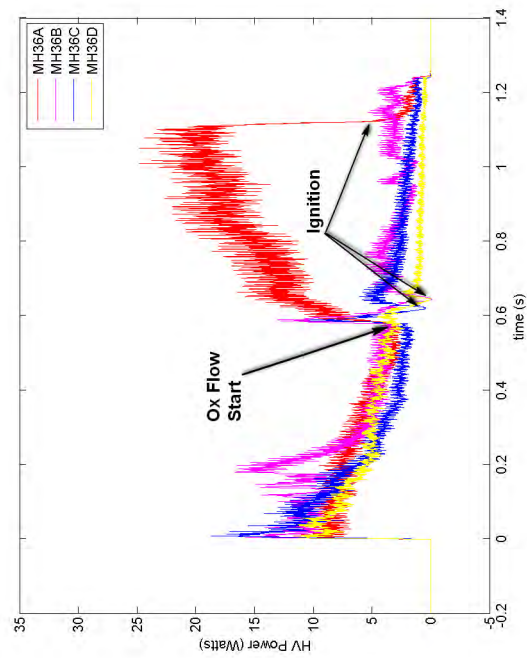
Fig. 3.12: MH36 Firing HVPS Data Plots

Table 3.11: MH34 Event Timing

	MH34A	MH34B	MH34C	MH34D	MH34E	MH34F	MH34G
Ox Feedline Pressure Rise	0.574	0.567	0.573	0.018	0.571	0.568	0.671
Ox Flow Start	0.569	0.284	0.567	0.169	0.565	0.561	0.665
Ignition	0.604	0.578	0.956	0.586	0.629	0.62	0.732
Steady State Start	5.511	0.671	0.746	0.715	0.772	0.788	0.881
Steady State End	6.06	1.434	1.364	1.434	1.365	1.36	1.468
Ox Feedline Depressurize	2.322	1.823	2.364	2.043	2.337	2.33	2.436
Flow End	1.556	1.434	1.571	1.579	1.566	1.572	1.688

Table 3.12: MH35 Burn Parameters

	MH35A	MH35B	MH35C	MH35D	MH35E
Average Oxidizer Feed Pressure (psia)	506.93	502.90	494.44	498.54	502.70
Average Oxidizer Mass Flow Rate (g/s)	5.67	5.84	5.45	5.53	5.91
Average Fuel Mass Consumption Rate (g/s)	1.13	1.15	1.12	1.04	0.80
Total Fuel Mass Consumption (g)	0.90	0.94	0.91	0.85	0.64
Average Mixture Ratio	5.03	5.07	4.85	5.30	7.36
Average Grain Regression Rate (mm/s)	1.90	1.26	0.98	0.79	0.55

Table 3.13: MH35 High Voltage Supply Parameters

	Pre-Flow Average Resistance (kOhm)	Ignition Peak Resistance (kOhm)	Post-Ignition Average Resistance (kOhm)
MH35A	193.0	153.6	NA
MH35B	20.4	148.7	NA
MH35C	39.8	145.7	NA
MH35D	45.3	29.8	NA
MH35E	14.0	41.2	NA

Table 3.14: MH35 Event Timing

	MH35A	**MH35B**	**MH35C**	**MH35D**	**MH35E**
Ox Feedline Pressure Rise	0.573	0.572	0.573	0.572	0.573
Ox Flow Start	0.567	0.566	0.567	0.566	0.568
Ignition	0.661	0.656	0.669	0.611	0.611
Steady State Start	0.779	0.735	0.826	0.817	0.738
Steady State End	1.363	1.372	1.372	1.378	1.366
Ox Feedline Depressurize	2.324	2.322	2.312	2.324	2.32
Flow End	1.546	1.549	1.553	1.558	1.542

Table 3.15: MH36 Burn Parameters Summary

	MH36A	**MH36B**	**MH36C**	**MH36D**
Average Oxidizer Feed Pressure (psi)	500	500	500	500
Average Oxidizer Mass Flow Rate (g/s)	5.86	5.86	5.85	3.41

Note: No feed transducer present, pressure estimated from pressure regulator guage

Table 3.16: MH36 High Voltage Supply Parameters

	Pre-Flow Average Resistance (kOhm)	Ignition Peak Resistance (kOhm)	Post-Ignition Average Resistance (kOhm)
MH36A	29.6	103.2	NA
MH36B	36.4	53.9	NA
MH36C	26.8	40.4	NA
MH36D	27.1	18.1	NA

Table 3.17: MH36 Event Timing

	MH36A	**MH36B**	**MH36C**	**MH36D**
Ox Flow Start	0.568	0.565	0.565	0.568
Ignition	1.127	0.612	0.604	0.631
Steady State Start	1.533	3.281	3.039	1.87
Steady State End	3.542	3.282	3.074	1.894
Ox Feedline Depressurize	4.236	4.276	4.268	4.159
Flow End	1.579	1.534	1.541	1.043

Chapter 4

Conclusion

In order to provide a "road map" to guide future designs, the following discussion centers on key 'lessons learned' during development of the electrostatic arc ignition concept. These lessons learned were used to develop the follow-on design as presented by Inkley, Whitmore, and Merkley [16].

4.1 Electrode Configuration

This study tested electrode and fuel grain configurations, including both concepts which attempted to arc through the oxidizer free stream (tests MH22 through MH24) as well as those which arced through the gas boundary layer along the surface of and ABS fuel grain (tests MH26 through MH36). Free stream arcing concepts necessarily require an insulating barrier between the high voltage and ground return sides of the spark path which has a higher electrical breakdown voltage than the free stream arc path during start-up oxidizer flow. Because conductive char plates all exposed interior motor surfaces during the shutdown transient, concepts which arc through the free gas stream were found to be prone to fouling of the electrode insulator after a small number of firings. This design caused misdirection of the spark along the insulator surface rather than through the free stream.

Spark electrodes configurations designed to cause intentional arcing through the gas layer along the grain surface were found to be the most effective way to consistently control the spark path in the soot rich environment of a hybrid motor. Additionally, such an electrode configuration are effective because the spark is placed to maximize initiation energy input to the interface between oxidizer and fuel, and to maximize the quantity of fuel ablated into the oxidizer. High voltage spark along the fuel grain was

shown to give highly reliable ignition. As discussed previously this concept has also since been successfully incorporated into the igniter for a 75mm grain, achieving reliable ignition.

4.2 Arcing Voltage

For reliable ignition, grain and electrode geometry should be designed to place the arc in a low flux area of the chamber. Effective electrical breakdown voltage across the arcing gap was shown to increase with increasing gas velocity. This effect was most pronounced for free stream arcing configurations, however was important even for surface arcing concepts. Electrode configurations in which the spark path must pass through the high velocity gas of the port were shown to increase the required breakdown voltage passed the point that will likely be prohibitive for implementation aboard flight systems.

Connected with the increase in breakdown voltage, mass flux, or its corollary gas velocity, was shown to be a limiting factor for the electrostatic arc ignition concepts tested here. Increasing the oxidizer mass flux at the spark location was shown to increase ignition latency. At the highest mass flux levels tested here, ignition would not occur.

Effective arc path resistance during arcing as well as breakdown voltage of the spark gap were shown to decease with successive burns, though the decrease after establishing a char layer on the grain surface during the first burn was most dramatic. It is likely that the arc does not travel continuously through the gas in the presence of conductive deposits on the grain surface but rather is made up of a string of many smaller arcs connected by conductive char 'islands' on the surface of the grain.

At the conclusion of this study additional research into the optimal initial grain surface preparation was needed, however, follow-on work performed at USU after the completion of this study shows promise. When printed using modern additive manufacturing processes like fused deposition modeling (FDM), ABS was found to posses a very unique electrostatic breakdown property. Although bulk ABS posses a very high electrical impedance, when additively manufactured as a layered surface, local surface structures resulting as an artifact of the manufacturing process were found to concentrate

charges along the deposited material layers when the material is subjected a high-voltage electrical potential field. These charge concentrations produced localized electrical arcing between material layers, allowing the material surface to break down at voltages significantly lower than would occur with a monolithically fabricated (extruded) fuel grain article. This follow-on work has shown that surface features associated with FDM type additively manufactured ABS grains make the pretreatment of the grain surface performed in this study unnecessary. Additionally, this special property of FDM printed ABS greatly reduces the required initial voltage to cause electrical breakdown. For the electrode and grain configurations tested in this study, the HVPS was required to produce sufficient voltage (many thousands of volts) to overcome higher initial burn arc path breakdown resistance while still maintaining sufficient current capability to deliver sufficient power once the arc path resistance decreases. The use of FDM printed grains allows the power supply to operate within more consistent load conditions over a series of ignitions and at much lower nominal operating voltages. Further research into the underlying principles governing the unique electrical breakdown properties of FDM printed ABS will allow for grain designs optimized for direct electrostatic arc ignition.

4.3   Demonstration of Electrostatic Arc Ignition Feasibility

The work presented here has demonstrated the feasibility of spark ignition of a gaseous oxidizer and solid fuel in a microhybrid motor. A small microhybrid was demonstrated to have restart capability up to 27 consecutive firings without replacing any components. Additionally the concept was miniaturized and successfully lit a larger hybrid motor four times without any component replacement or refurbishment, showing the viability of the igniter for systems requiring restartablility. Total number of ignitions was shown to be limited only by the quantity of fuel available in the igniter.

In addition, a large body of data was collected characterizing the required power, voltage, and total energy input for ignition. Electrostatic arc ignition for hybrid motors was shown to be feasible in the low energy input range of 20- to 50 W using total energy of less than 10J. In a small form factor this power input was amplified to a total igniter

power output of approximately 50,000 W.

4.4 Applications for This Work

The research presented here formed the basis for follow-on research which developed a highly successful mid-sized hybrid motor igniter which was fully integrated in the the main flow path of 75mm and 98mm motors. Key contributions from this work include the development of the surface arcing fuel grain concept, demonstration of the importance of spark location in low flux regions of the motor head end, and the sizing of a DC HVPS.

This igniter concept is especially promising for realizing the full safety and simplicity benefits of hybrid rocket motors. Current state of the art ignition systems for hybrid motors continue to require reactants distant from the main propellants. In many cases this may invalidate the safety advantages which motivate the use of hybrid motors by introducing disadvantages associated with traditional liquid or solid propellant systems. Electrostatic arc ignition is an enabling technology, allowing for hybrid motors with restart capability without the need to carry reactive components distinct from the main propellants. Additionally, the direct ignition microhybrid motor concept may hold promise as a standalone miniature propulsion system for small satellites.

References

[1] Wheelock, V. and Kraemer, R., *Rocketdyne: Powering Humans into Space*, AIAA Education, Reston, VA, 2006.

[2] Barrett, D. H., "NASA SP-8051 :Solid Rocket Motor Igniters," *NASA Space Vehicle Design Criteria*, 1971.

[3] Huzel, D. K. and Huang, D. H., *Modern Engineering for Design of Liquid-Propellant Rocket Engines*, American Institute of Aeronautics & Astronautics, Reston, VA, 1992.

[4] Sutton, G. P. and Biblarz, O., *Rocket Propulsion Elements*, John Wiley & Sons, Inc., New York, 7th ed., 2001.

[5] Karabeyoglu, A., Stevens, J., Geyzel, D., Cantwell, B., and Micheletti, D., "High Performance Hybrid Upper Stage Motor," *47th AIAA/ASME/SAE/ASEE Joint Propulsion Conference & Exhibit*, July 2011, pp. 1–24.

[6] Department of Defense, "General Requirements for Preclusion of Ordnance Hazards in Electromagnetic Fields," Tech. Rep. MIL-STD-1385B, U. S. Navy, Naval Sea Systems Command, Washington, DC, 1986.

[7] Alliant Techsystems Inc., "ATK Space Propulsion Products Catalog," 2008.

[8] United States Air Force, "Effectiveness of the Minuteman II Stage III Refurbishement Program," Tech. Rep. January, 1985.

[9] Caveny, L. H. and Summerfield, M., "Micro-Rocket Impulsive Thrusters," Tech. Rep. AMS 1014, Princeton University, Department of Aerospace and Mechanical Sciences, Princeton, NJ, 1971.

[10] Bastian, T. W. and Roberts, J. S., *Multi-Burn Solid Fuel Restartable Rocket and Method of Use*, U.S Patent 4,357,795, Nov. 9, 1982.

[11] Nufer, B. M. K. S. C., "A Summary of NASA and USAF Hypergolic Propellant Related Spills and Fires," Tech. Rep. June, National Aeronautics and Space Administration, NASA/TP-2009-214769, Florida, 2009.

[12] ITB Inc, "Technology Evaluation for Environmental Risk Mitigation Principal Center - Hypergolic Propellant Destruction Evaluation: Cost Benefit Analysis," Tech. Rep. August, National Aeronautics and Space Administration, 2010.

[13] Tiliakos, N., Tyll, J., Herdy, R., Sharp, D., Moser, M., and Smith, N., "Development and Testing of a Nitrous Oxide/Propane Rocket Engine," *AIAA Joint Propulsion Conference*, 2001.

[14] Mueller, J., "Thruster Options for Microspacecraft: A Review and Evaluation of Existing Hardware and Emerging Technologies," *American Institute of Aeronautics and Astronautics*, 1997, pp. 1–29.

[15] Bombelli, V., Simon, D., Moerel, J.-L., and Marée, T., "Economic Benefits of the Use of Non-Toxic Mono-Propellants for Spacecraft Applications," *39th AIAA/ASME/SAE/ASEE Joint Propulsion Conference and Exhibit*, American Institute of Aeronautics and Astronautics, Reston, Virigina, July 2003.

[16] Whitmore, S. A., Peterson, Z. W., and Eilers, S. D., "Deep Throttle of a Nitrous Oxide and Hydroxyl-Terminated Polybutadiene Hybrid Rocket Motor," *Journal of Propulsion and Power*, Vol. 30, No. 1, Jan. 2014, pp. 78–86.

[17] Whitmore, S. A. and Peterson, Z. W., "Closed-Loop Precision Throttling of a Hybrid Rocket Motor," *Journal of Propulsion and Power*, Vol. 30, No. 2, March 2014, pp. 325–336.

[18] Eilers, S. D., *Development of the Multiple Use Plug Hybrid for Nanosats (Muphyn) Miniature Thruster*, Phd thesis, Utah State University, 2013.

[19] Whitmore, S. A., Sobbi, M., and Walker, S., "High Regression Rate Hybrid Rocket Fuel Grains with Helical Port Structures," *50th AIAA/ASME/SAE/ASEE Joint Propulsion Conference*, American Institute of Aeronautics and Astronautics, Reston, VA, July 2014.

[20] Cantwell, B. and Karabeyoglu, A., "Recent Advances in Hybrid Propulsion," *International Journal of Energetic Materials and Chemical Propulsion*, Vol. 9, No. 4, 2010, pp. 305–326.

[21] Goff, J. A. and Cross, M. C., "HatchBasket System for ISS-Enabled SmallSat Deployments and Externally-Hosted Tech Demo Payloads," *28th Annual AIAA/USU Conference on Small Satellites*, Vol. c, Logan, UT, 2014, pp. 1–9.

[22] London, J. R. I. I. I., Marley, A. B., and Weeks, D. J., "Army Nanosatellite Technology Demonstrations For The Tactical Land Warfighter," Tech. Rep. 256, US Army Space and Missile Defense Command, Redstone Arsenal, AL, 2010.

[23] Annon, "Federal Business Opportunities," [https://www.fbo.gov/index?s=opportunity&mode, Accessed 1/6/2014].

[24] Whitmore, S. A. and Peterson, Z. W., "Analytical and Experimental Comparisons of HTPB and ABS as Hybrid Rocket Fuels," *47th AIAA/ASME/SAE/ASEE Joint Propulsion Conference & Exhibit*, 2011, pp. 1–48.

[25] ALTMAN, D., "Hybrid Rocket Development History," *27th Joint Propulsion Conference*, American Institute of Aeronautics and Astronautics, Reston, VA, June 1991.

[26] Annon, "SpaceX Updates," [http://www.spacex.com/updates_archive.php?page=0205-0505, Accessed 1/6/2014].

[27] Young, A., *The Saturn V F-1 Engine: Powering Apollo Into History*, Springer Science & Business Media, New York City, NY, 2008.

[28] Wilson, M., "Catalytic Decomposition of Nitrous Oxide Monopropellant for Hybrid Motor Ignition," American Institute of Aeronautics and Astronautics, MS Thesis, Utah State University, July 2013, pp. 1–116.

[29] Jacobsen, L. S., Carter, C. D., Baurle, R. a., Jackson, T. a., Williams, S., Bivolaru, D., Kuo, S., Barnett, J., and Tam, C.-J., "Plasma-Assisted Ignition in Scramjets," *Journal of Propulsion and Power*, Vol. 24, No. 4, July 2008, pp. 641–654.

[30] Voris, C. R., Smith, B., Williams, N., Miller, J., Ralston, J., Richardson, J., Moore, W., Doll, D., Maughn, J., and Hayes, F., "Block II SRM Conceptual Design Studies Final Report," Tech. Rep. NASA-CR-179048, 1986.

[31] Inkley, N. R., "Power Efficient Restart-Capable Acrylonitrile Butadiene Styrene-Based Arc Ignition For Hybrid Rocket Motors," MS thesis, Utah State University, 2013.

[32] Annon, "Jacob's Ladder and Singing Plasma Arc," [http://www.amazing1.com/jacobs-ladder.html, Accessed 1/6/2014].

[33] Annon, "NI CompactDAQ," [http://www.ni.com/data-acquisition/compactdaq/, Accessed 1/6/2014].

[34] McBride, B. and Gordon, S., "Computer Program for Calculation of Complex Chemical Equilibrium Compositions and Applications II. Users Manual and Program Description," *NASA RP-1311*, 1996.